Modeling Piston Secondary Motion and Skirt Lubrication with Applications

by

Pasquale Totaro

B.Sc., Energy Engineering
Politecnico di Milano, 2012

MASSACHUSETTS INSTITUTE
OF TECHNOLOGY
AUG 15 2014
LIBRARIES
ARCHIVES

Submitted to the Department of Mechanical Engineering in Partial Fulfillment of the Requirement for the Degree of Master of Science in Mechanical Engineering

at the

Massachusetts Institute of Technology

June 2014

© 2014 Massachusetts Institute of Technology. All rights reserved.

Signature of Author ________ Signature redacted
Department of Mechanical Engineering
May 09, 2012

Certified by ____________ Signature redacted
Tian Tian
Principle Research Engineer, Department of Mechanical Engineering
Thesis Supervisor

Accepted by ____________________ Signature redacted
David E. Hardt
Chairman, Department Committee on Graduate Studies
Department of Mechanical Engineering

Modeling Piston Secondary Motion and Skirt Lubrication with Applications

by

Pasquale Totaro

Submitted to the Department of Mechanical Engineering on May 09, 2014
in partial fulfillment of the requirements for the degree of
Master of Science in Mechanical Engineering

Abstract

The interest in reducing emission and improving engine efficiency has become a major push in industry, due to upcoming stricter regulations. A great deal of attention has been given to the frictional losses due to piston and liner interaction, as they represent a significant portion of the total mechanical losses.

This thesis work focuses on further development and application of an existing model for the piston's secondary motion and skirt lubrication.

Model development has been focused on introducing liner dynamic deformation, temperature and shear-thinning effect on viscosity, and arbitrary skirt's shape definition. The theory behind the inclusion of these components is discussed and the modifications to the existing model are explained.

In regards to the model's applications, an important topic is the model validation, for which friction results from simulations are compared with experimental results obtained on a floating liner engine. The analysis covers the running condition of 1000 rpm, at partial and full load. This study is, however, not concluded and more cases need to be studied in order to complete the validation of the model.

The second application focuses on the effects of geometrical patterns on the skirt on friction and secondary motion of the piston. First, some regular patterns were studied and found to have negative effects on friction due to their inability to build sufficient hydrodynamic pressure, compared to the baseline design. Then, a different sets of patterns were proposed to more effectively utilize available oil and to maximize the hydrodynamic pressure generation in the skirt region. The results show that new strategy can significantly reduce friction of the skirt without introducing negative impact on the secondary motion.

This thesis work aims to make the model a more complete and powerful tool to understand piston's secondary motion and the applications are meant to show the capabilities of the model, as an instrument to approach piston's design and inspire new ways and ideas to reduce frictional losses.

Thesis Supervisor: Dr. Tian Tian
Title: Principle Research Engineer, Department of Mechanical Engineering

Acknowledgements

It really feels like just few months has passed since I started the Master program here at MIT. Time has gone by so fast that these two incredible years seem blended in a concentrated, colorful and delicious sip of experiences. The days I spent here and the people I met have made this an amazing chapter of my life.

First of all, I would like to thank my supervisor Dr. Tian Tian, for the incredible support he has provided to my work and for the opportunity he gave me to express my personality in the research I do. I would also like to thank my labmates Eric Zanghi, Camille Baelden, Yang Liu, Mathieu Picard, Tianshi Fang, Qing Zao, Dr. Dallwoo Kim, Zachary Westerfield, Renze Wang, Dr. Eric Senzer and Dr. Kai Liao for sharing their experiences and knowledge with me and for making working much more enjoyable and intriguing.

I also have a lot of appreciation for the support given by the consortium on lubrication in internal combustion engines with additional help by Argonne National Laboratory and the US department of energy. I want to thank Daimler, Mahle, PSA Peugeot Citroën, Renault, Shell, Toyota, Volkswagen, Volvo Cars, and Volvo Truck, and more specifically their representatives Rolf-Gerhard Fiedler, Hans-Jurgen Fuesser, Matthias Martin, Remi Rabute, Bengt Ol-son, Paulo Urzuá Torres, Bogdan Kucinschi, Scott Rappaport and Steven Przesmitzki for their encouragement and fruitful suggestions.

Lastly, I am really grateful for the time I spent with my friends and fellow students Mark, Levi, Tim, Eric and David and for the constant warming support I receive from my family and my lifelong friends Antonio P., Antonio S., Alessandro S., Antonio C. and Marco P., which make thousands of kilometers of distance feel just like a couple of blocks.

List of Figures

2.1 Power cylinder system 18

2.2 Side Force 19

2.3 Primary and Secondary motion 20

2.4 Bearings 21

2.5 Liner cold deformation 22

2.6 Piston cold shape 23

2.7 Piston and Liner thermal deformation 24

2.8 Oil visualization in skirt area 26

2.9 Oil flow at the skirt's boundary 27

2.10 Oil film thickness at the start of calculation 28

2.11 Oil film thickness during compression stroke 28

2.12 Oil supply to the system 29

2.13 Newton's iterative solving scheme 31

2.14 Liner compliance matrix isolation 33

2.15 Oil viscosity data fitting 34

2.16 Modification of the hydrodynamic solver 36

2.17 Cells definition in the calculation domain 39

2.18 Skirt input data 42

2.19 Convex boundary detection 43

2.20 Example point cloud transformation 44

2.21 Example of boundary calculation 45

3.1 Floating Liner Engine schematic 47

3.2 Stretching and compression of piezoelectric sensors 48

3.3 Sensors' behavior during down-stroke 49
3.4 Sensors' behavior during up-stroke 50
3.5 Friction measured by the sensors 50
3.6 Friction measurement's variation 51
3.7 Simulated cases 53
3.8 Engine's data 53
3.9 Friction comparison, 2 bar IMEP, constant viscosity 54
3.10 Total And hydrodynamic friction comparison 55
3.11 Friction comparison, 2 bar IMEP, HTHS 2.9 oil 56
3.12 Average viscosity, expansion stroke 57
3.13 Comparison with estimated piston's friction, 2 bar IMEP 58
3.14 Friction comparison, 4 bar IMEP, HTHS 2.9 oil 59
3.15 Comparison with estimated piston's friction, 4 bar IMEP 60
3.16 Lateral motion trend comparison, intake stroke 62
3.17 Lateral motion trend comparison, compression stroke 63
3.18 Lateral motion trend comparison, expansion stroke 63
4.1 Piston's skirt pattern 66
4.2 Patterns with different features' size 68
4.3 Skirt's center cross section 69
4.4 Skirt FMEP comparison – baseline and dots pattern 70
4.5 Friction comparison – baseline dots pattern 71
4.6 Dots patter – solid to solid contact 71
4.7 Baseline piston – hydrodynamic pressure distribution 72
4.8 Dots pattern – hydrodynamic pressure distribution 73

4.9 Lateral motion and tilt angle comparison 74

4.10 Inertia and force comparison 75

4.11 Skirt FMEP comparison – baseline, voids and rows 76

4.12 Average fully flooded regions – baseline, voids and rows 77

4.13 Oil paths – dots, voids and rows features 78

4.14 Oil supply to skirt from liner 81

4.15 usual skirt profile 82

4.16 New pattern's schematic 82

4.17 Feature's profile and cross-section 83

4.18 Skirt profile with the application of the new pattern 84

4.19 Friction force comparison – Racing engine 84

4.20 Comparison of hydrodynamic pressure generated – TH 85

4.21 Comparison of hydrodynamic pressure generated – ATH 86

4.22 Friction force comparison – optimized pattern 87

4.23 Pattern's friction force comparison – intake stroke 87

4.24 Friction force comparison – passenger car engine 88

4.25 New pattern's alternatives 89

4.26 Piston's secondary motion comparison 90

4.27 Comparison of average oil film thickness in the chamfer 91

Contents

1 Introduction

1.1 Project Motivations 14

1.2 Thesis Work 15

2 Development on previous model

2.1 Introduction to Power Cylinder System 18

2.2 Existing model 20

2.3 Liner dynamic deformation 29

2.4 Shear-thinning and temperature effect on viscosity 33

2.5 Arbitrary skirt domain definition 42

3 Comparison of model's results with experimental results

3.1 Floating Liner set-up description 47

3.2 Friction results comparison 52

3.3 Secondary motion trend estimation 61

4 Piston's skirt patterns analysis

4.1 Skirt patterns 66

4.2 Skirt FMEP results from the model 67

4.3 New pattern design – Racing engine 79

4.4 New pattern design – Passenger car engine 88

5 Conclusion

5.1 Development and application of the model 93

5.2 Future work 94

Chapter 1

Introduction

1.1 Project Motivations

Internal combustion engines have heavily changed our life ever since their invention. Every day in our usual routine one or more of our actions is made possible or easier thanks to the use of this technology. During many years internal combustion engines have become more sophisticated and their usage has widely spread and increased in the transportation system and industry. Since 1890, when the internal combustion engine industry was effectively founded, only 50,000 engines were sold [1]; in the 2013 the units sold have been 15 million.

The usage of IC engines is however strictly correlated with concerns about CO_2 and pollutants release in the atmosphere, and the standards regulating emissions are becoming stricter and stricter. In the 2012, in the United States, the EPA (Environmental Protection Agency) has set a limit of *263 g/mi* on carbon dioxide emission corresponding to *27.3 mpg* of fuel economy for passenger cars [2]. The long term plan is however to further decrease emission by *31%* by 2020 [3].

In this scenario a lot of efforts are put into research to improve the design of engines and meet the standards. In particular a lot of attention is given to mechanical frictional losses, which approximately account for *10%* of total energy losses. Among these, *40–55%* are observed in the power cylinder system, made up of piston (*25-47%*), ring-pack (*28-45%*) and connecting-rod bearings (*18-33%*) [4].The potential that this system has to improve is the motive that has encouraged this thesis work.

One dominating phenomenon in the power cylinder system is the piston-liner interaction. This interaction can be described by studying piston's secondary motion and lubrication, which is the main topic of this project. A comprehensive understanding of this motion is extremely useful to study how the design of pistons affects the frictional losses, wear, oil consumption, engine noise and reliability.

This thesis focuses on the further development of the piston's secondary motion and lubrication model, already built during the progress of this project, and will also address model validation and interesting applications.

1.2 Thesis Work

The existing model, first developed by Dongfang Bai [4], has set a good and comprehensive basis to study piston's secondary motion, but the further development of it is necessary as some physical phenomena occurring in the system are not yet represented, some assumptions needs to be relaxed and the code has not been used previously to study real cases or address real problems.

The development of the model is discussed in Chapter 2 of this thesis. The first issue addressed is the introduction of liner dynamic deformation. The dynamic deformation is defined as the deformation due to the interaction between piston and liner, or more practically the deformation due to the force that the piston applies on the liner. As it will be discussed in more details, the existing version of the model only included the skirt's dynamic deformation, assuming the liner a rigid component. This assumption, however, may not be a good approximation; in fact, the liner can be rather flexible in some regions, and deform as much as the skirt does. Furthermore, the assumption of rigid liner makes it easier for the piston to enter in solid to solid contact with the liner, affecting the final results of friction force.

The second important introduction in the code is the consideration of temperature and shear-thinning effect on viscosity. The existing version of the model considers a constant and unique value of viscosity for the whole calculation, but this can prevent the results to be realistic. Usually the temperature along the liner can vary from *130-110 °C* at TDC and *80-90 °C* at BDC, and also the local shear rate at which the oil is subject in the skirt region can change depending on piston's speed, oil feel thickness and side force. These phenomena can change the viscosity by order of magnitude and therefore affect the results of the model.

Another major modification to the model regards the structure of the calculation domain. The calculation domain for the skirt region, used in the existing model, it has been assumed rectangular for both thrust side and anti-thrust side. Generally, however, the skirt is not rectangular, and the thrust and anti-thrust side can also be different. This has been taken into account and the possibility to define an arbitrary and different domain geometry for thrust and anti-thrust side has been introduced.

A big part of this thesis work has also been the direct application of the model. One important application regards the simulation of engine's cycles based on the Floating Liner Engine. The Floating Liner Engine is an experimental set-up in our lab, through which it is possible to measure the instantaneous friction force. The main purpose of this study is to compare the friction force calculated and experimentally measured, in order to analyze the accuracy of the model.

A second, really interesting, application of the model, it has been studying the effect of graphite patterns on the piston's skirt. Several prototypes have been analyzed, finding a physical explanation to the resulting frictional losses calculated. Since none of the patterns has resulted to give less frictional losses when compared to a baseline piston, a new pattern has been designed from scratch and tested, reporting interesting improvements in performances.

As a conclusion, in Chapter 5, the main achievements made in this thesis are summarized and suggestions to contribute to this project in the future are discussed.

Chapter 2

Developments on previous model

2.1 Introduction to power cylinder system

The first thing that needs to be introduced, in order to understand the content of this thesis, is the mechanical system that has been modeled, highlighting key components and concepts.

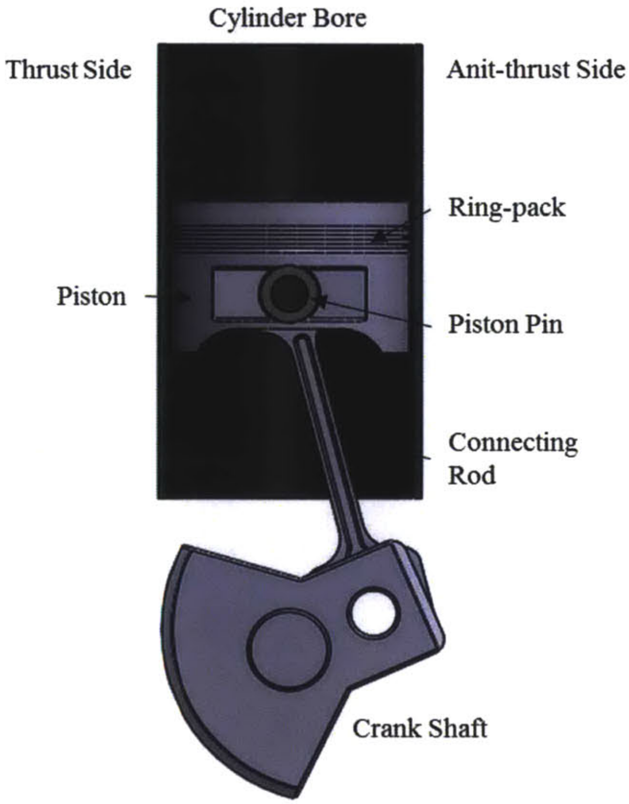
Cylinder Bore
Thrust Side
Anit-thrust Side
Ring-pack
Piston
Piston Pin
Connecting Rod
Crank Shaft

Figure 2.1 – Power cylinder system

Figure 1 shows a simplified representation of the system. The piston has the role of transferring the energy released by the combustion to the crank shaft. The combustion chamber pressure, however, due to the geometry of the system, will cause a side force that pushes the piston towards the liner, as showed in Figure 2.

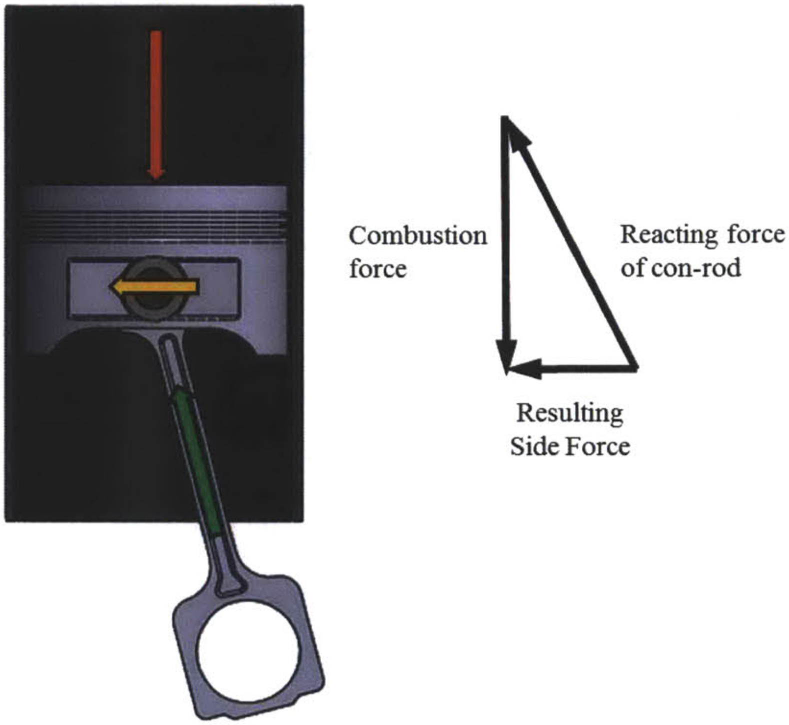

Figure 2.2 – Side Force

The side force is the cause of the so called secondary motion of the piston. This motion can be decoupled in two main components: lateral motion and tilting motion. As shown in Figure 3, the first describes the pure translation of the piston in the radial direction, the second describes the relative rotation of the piston around the pin. Along with these definitions, it is usually also made a distinction between the two skirt's sides of the system: it is called thrust side, the side of the system towards which the piston is pushed during the expansion stroke, whereas the anti-thrust side is the opposite side. This is an important distinction to keep in mind when designing pistons, in fact, usually the skirt geometry is different from side to side.

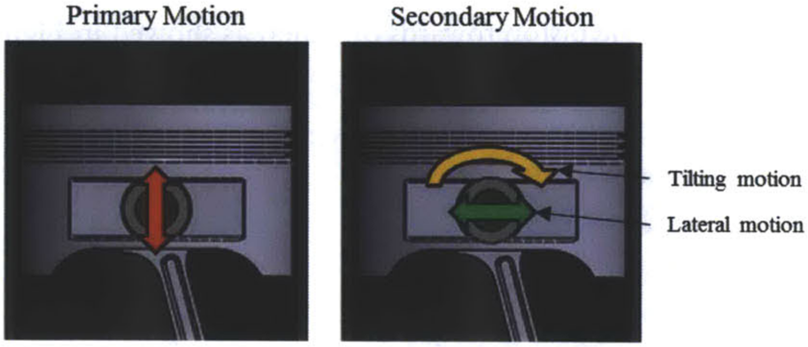

Figure 2.3 – Primary and Secondary motion

The first part to model, in order to describe the piston's secondary motion, is the dynamics of the system (described in detail in Chapter 2 of [4]), which describes the primary motion of the piston and the forces acting on it. This is, however, not the most complicated part to understand. The secondary motion and lubrication is, in fact, also largely influenced by the amount of lubricant available to the skirt at any instant. To study this phenomenon it is critical to take track of the oil on the liner and in the skirt's region. The details describing the modeling of oil transport between skirt and adjacent areas are widely explained in Chapter 3 and 4 of Bai's thesis [4], in this thesis the discussion will be limited to describe capability, assumptions and improvements done on the existing model.

2.2 Existing model

The development of the piston secondary motion model is the result of the modeling work done over the years [4, 5, 9]. Also experimental observations from the 2D LIF engine [6, 7, 8] have helped the development of the oil lubrication sub-model in the existing model. This section will summarize the work done and discuss the further developments.

The first part to analyze is the dynamics sub-model, which is fairly easy to solve [4]. The assumptions done in this part are not too many, but it is useful to list them, as they could be topics of further work in the future. A first simplification made to solve the motion of the piston is the assumption of no friction at the connecting rod bearing and at the pin bosses. The first hypothesis is close to reality and its influence to the motion is negligible. On the other hand, the pin lubrication is a subtle phenomenon. The assumption of no friction at the pin bosses requires the pin and piston to be perfectly lubricated, assuming that no solid to solid contact takes place, however, this may not be the case. In fact, when the piston is subject to important inertial forces, the friction at the pin bosses can be significant and the tilting motion can be affected by the motion and rotation of the connecting rod, especially between strokes, when the side force changes sign, and the interaction between piston and liner is limited. On the other hand, modeling the lubrication between piston and pin is a really complicated problem and it is been currently neglected in this model [17]. Nonetheless, it could be an interesting topic to work on in the future, in order to improve the model.

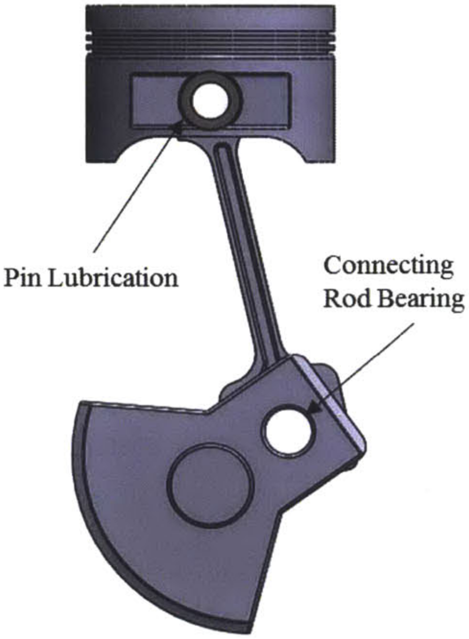

Figure 2.4 – Bearings

Another important topic to discuss is the deformations taking place into the system. The only components for which deformations are taken into account are piston and liner. We can divide the deformations in three groups: cold, thermal and dynamic deformations. The cold deformations are considered those caused by particular constrains in the power cylinder block or by manufacturing process. Specifically for the liner, the ideal shape is different from the real one because of static stresses introduced when assembling the whole engine block (Figure 5), whereas for the piston, its manufacturing process defines the profile of the skirt for lubrication purposes (Figure 6).

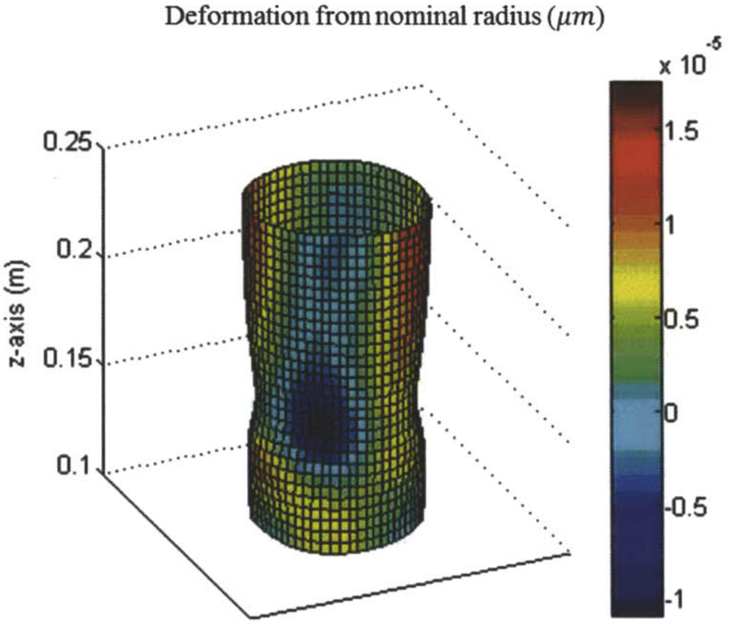

Figure 2.5 – Liner cold deformation

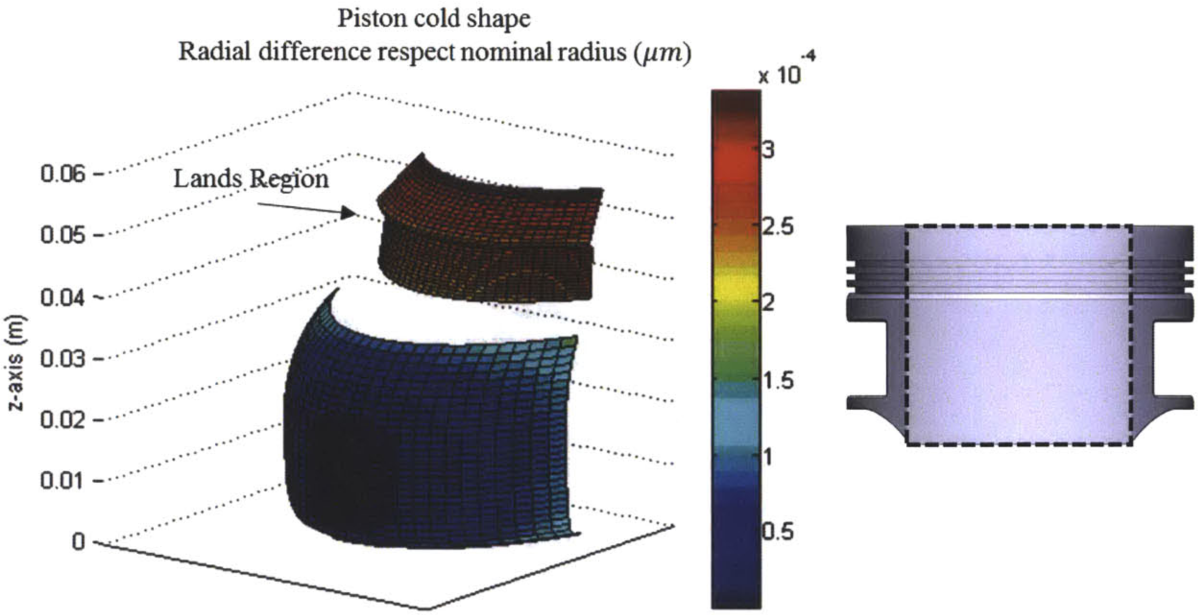

Figure 2.6 – Piston cold shape

The second type of deformations are thermo-mechanical and are due to the temperature rise of the components. The piston's deformation is usually greater at the crown, usually reaching values between $200 - 250\ \mu m$. The liner's deformation depends on the way the component is connected to the engine's head and can usually reach values between $80 - 120\ \mu m$. The magnitude of radius increase due to thermal-mechanical stresses is usually greater that the cold clearance and needs to be considered in the model.

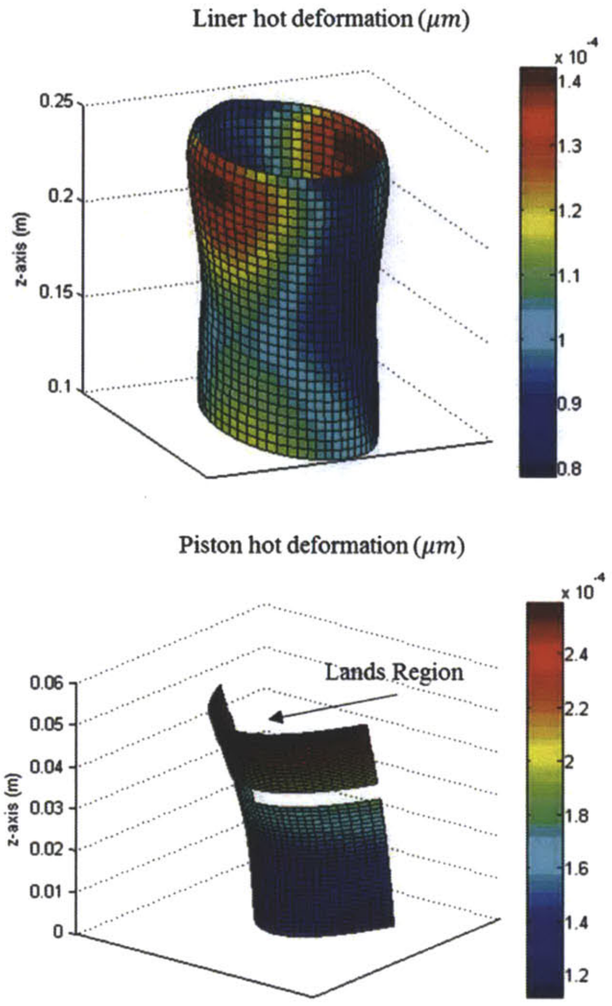

Figure 2.7 – Piston and Liner thermal deformation

As determinant as thermal stresses are dynamical stresses due to piston-liner interaction and chamber pressure. In the existing model dynamical deformations are only considered for the piston; these includes deformations due to piston-liner interactions, inertial forces and chamber pressure, with the first being the most important. Usually the side force can reach values of thousands of Newton, even for passenger cars, and this would cause the piston to deform substantially. The deformation are determined using a compliance matrix, which is an input obtained with appropriate FEA models. Differently from the pistons, the liner is considered rigid in the existing model. This might be not a good approximation in those cases where the liner is rather flexible and deform with a magnitude comparable to the skirt when interacting with it. This assumption has been relaxed in the current version of the model and the approach used is described in Section 2.3.

The last part to discuss is the hydrodynamics and lubrication model. Physically, any mechanism that can influence the oil motion is described, in fact, pressure and inertia driven flow are calculated, as well as Couette flow [10, 4]. The oil film thickness is calculated at every calculation step, for every point in the calculation domain, once the boundary conditions are defined. This represents an important difference with other models [15,16], which either assume constant oil film thickness or constant boundary condition. As shown in Figure 8, oil is free to be attached with skirt or liner, so that it is possible to realistically describe fully flooded and partially flooded regions. The surface tension is not taken into account in the model, therefore the amount of oil, at a specific point in the domain, is empirically associated half with the liner, half with the piston. This is an aspect that can be improved. The boundary conditions are partial calculated, partially pre-determined. In order to explain this part of the model, the calculation process will be quickly introduced.

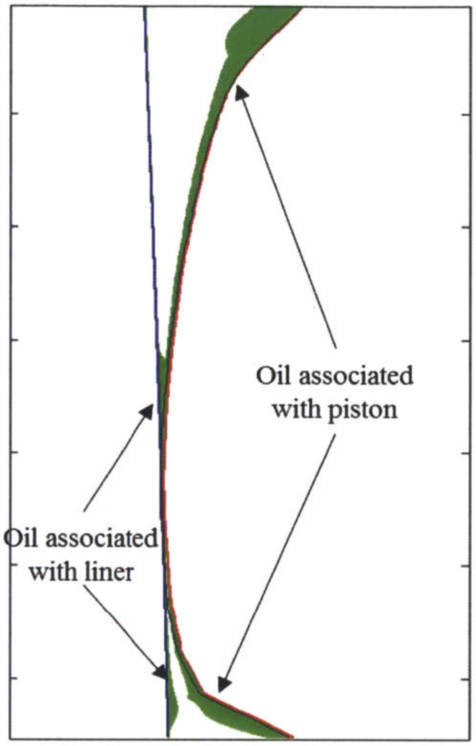

Figure 2.8 – Oil visualization in the piston-liner interface at central section of the skirt, thrust side

- The first step to start the calculation is to define the initial oil amount in the system, namely in the skirt and liner region, at the beginning of an intake stroke (Figure 2.10, left).

- Once the simulation begins, the oil film thickness in the system will be purely defined by dynamics and hydrodynamics (Figure 2.10 and 2.11). As the piston starts the stroke, oil will enter the bottom of the skirt since scraped from the liner (Figure 2.10). At the same time oil will be accumulated below the oil control ring, as it is assumed that no oil can reach the ring pack. This is good approximation as the oil control ring allows much less oil to pass through on the liner than the piston's skirt. A certain amount of oil may also enter the oil control ring groove and be drained through the drain holes. The significance of this oil release depends on the oil supply rate to the liner region below the skirt and will be a subject for future investigations. Currently, the oil accumulated in the piston's chamfer during a down-stroke is stored and will become a source of oil supply during the following up-stroke.

- Once the piston reaches BDC, it will start its upstroke and the oil exiting the lower boundary of the skirt is supposed to stay on the liner and is recorded as part of the oil supply available to the piston for the following down-stroke.
- Once the piston reaches TDC, the oil film thickness calculated on the portion of the liner below the piston is increased by a constant value to model oil supply to the system, and it will represent the lower boundary condition for the skirt, during the following down-stroke (Figure 2.12, left).

This is a crude way to practically represent the oil droplets coming from various interactions below the piston's skirt. How oil can flow to the liner, below the piston's skirt area, depends on the design of the crank shaft (wet or dry sump) as well as the oil cooling jets. This is also a subject for future investigations. Note that oil can also escape the skirt from the sides by means of pressure driver flow, as the side boundary pressure is assumed atmospheric (Figure 2.9).

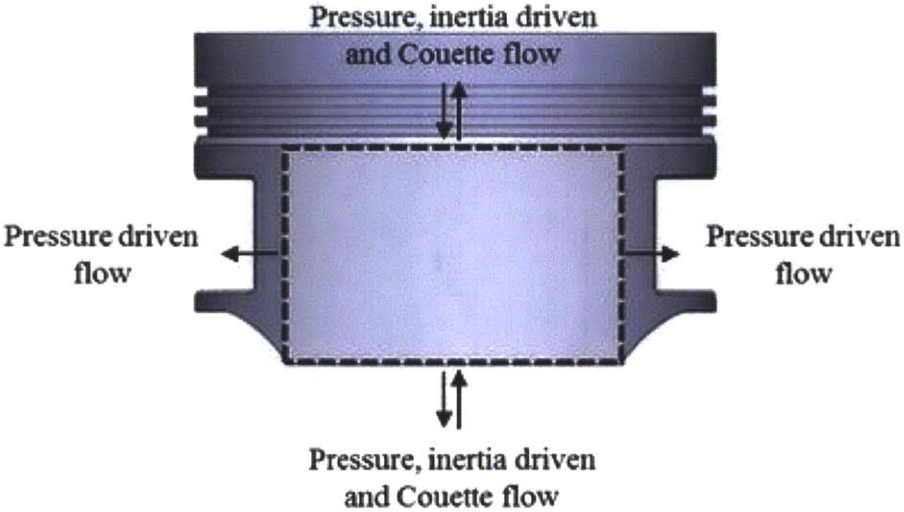
Pressure, inertia driven and Couette flow
Pressure driven flow
Pressure driven flow
Pressure, inertia driven and Couette flow

Figure 2.9 – Oil flow at the skirt's boundaries

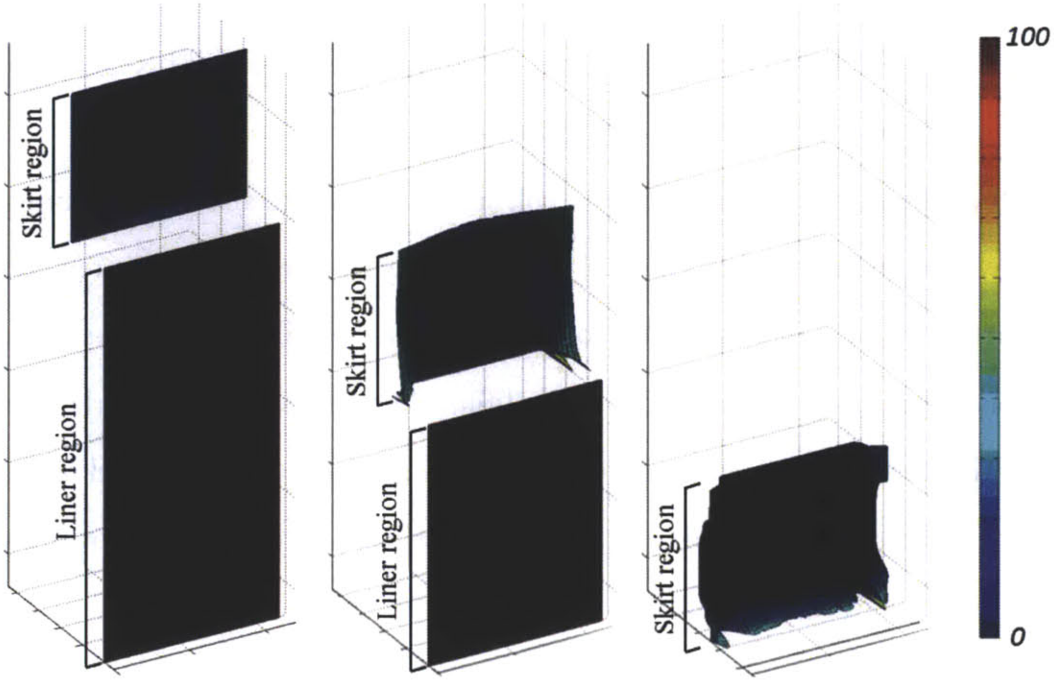

Figure 2.10 – Oil film thickness distribution on liner in microns
Start of calculation – Intake stroke – Thrust side

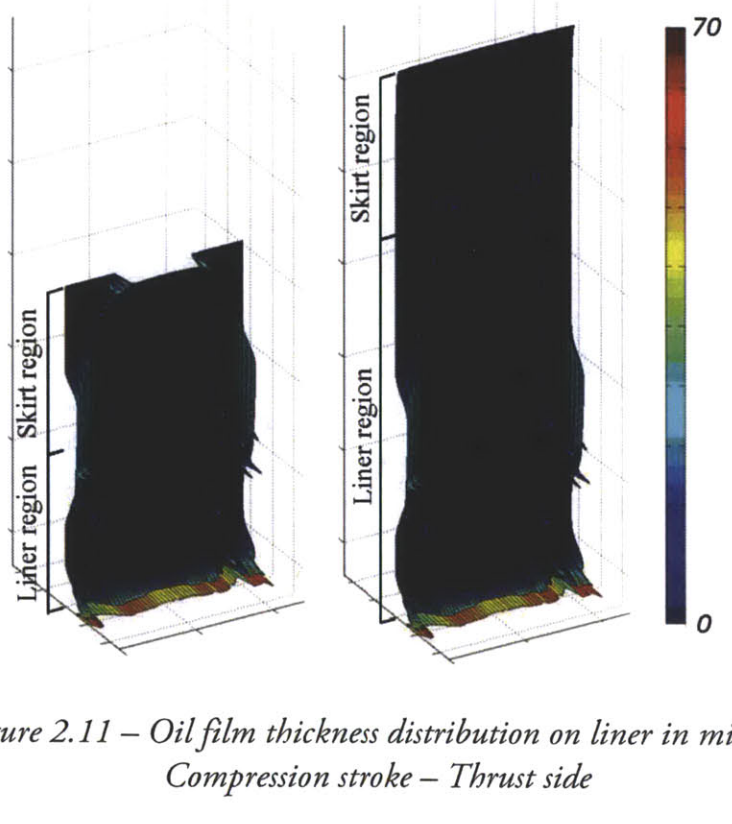

Figure 2.11 – Oil film thickness distribution on liner in microns
Compression stroke – Thrust side

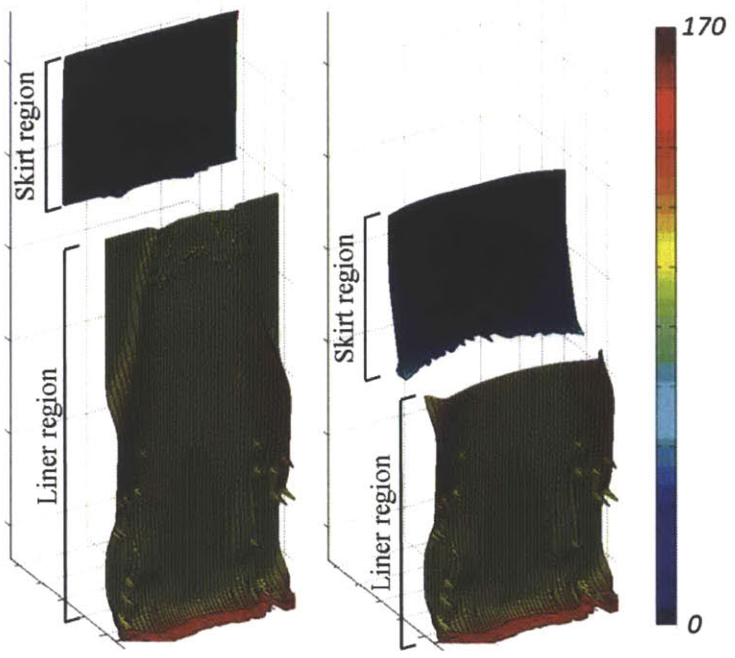

Figure 2.12 – Oil film thickness distribution on liner in microns
Oil supplied on the liner region - Expansion stroke – Thrust side

In summary, the oil film thickness and boundary conditions in the system, except that for the initial condition, are always calculated. The hydrodynamic is well described in the model, the only thing that needs to be improved, is the way oil supply to the system is defined.

2.3 Liner dynamic deformation

As already introduced in the previous sections, the liner dynamic deformation was a missing part in the existing model and it has been implemented in the model in this work. In order to comprehend this topic, the numerical-iteration process used to solve the secondary motion needs to be briefly described.

The first step in the simulation process is to calculate the primary motion of the piston. This only depends on the geometry of the components and on the set speed, therefore it is straightforward to achieve. Once the side force, the piston vertical position, velocity and acceleration have been determined, it is necessary to determine the lateral displacement and tilt of the piston, dynamic deformation of the components, hydrodynamic and solid to solid contact pressure distribution over the skirt region, and instantaneous clearance volume. Most of these variables are interconnected. For example in order to determine the pressure distribution in the skirt region, the clearance volume needs to be known; however, the clearance is affected by secondary motion and dynamic deformations, which themselves are influenced by the pressure distribution. To solve such a problem it is necessary to guess the value of a group variables, calculate the others and correct the guess. This process has to be repeated until the value of the variables satisfy a system of equations, which in this case is represented by the force and torque balance equations on the piston.

The specific process is summarized in Figure 2.13. The lateral displacement, tilt and dynamic deformations are variable for which, at the first iteration, the value is guessed. Once these variables are fixed, the clearance is determined and the pressure distribution can be found, solving the hydrodynamics of the system.

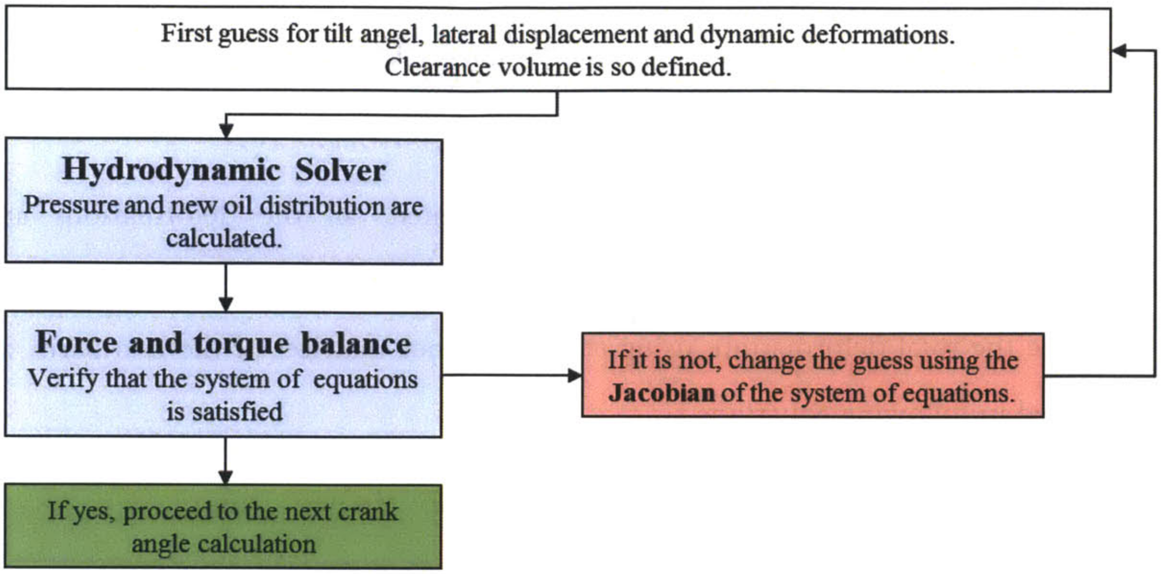
First guess for tilt angel, lateral displacement and dynamic deformations.
Clearance volume is so defined.
Hydrodynamic Solver
Pressure and new oil distribution are calculated.
Force and torque balance
Verify that the system of equations is satisfied
If it is not, change the guess using the **Jacobian** of the system of equations.
If yes, proceed to the next crank angle calculation

Figure 2.13– Newton's iterative solving scheme

Once the hydrodynamic solver has generated a solution for the pressure distribution, the force and torque balance equations for the piston are verified. If the system of equations is satisfied, the calculation for that specific crank angle is completed; if not, the Jacobean of the system (which will be described in more details in the next section) is used to change the initial guess.

In this iterative process, the dynamic deformations (d) are first assumed absent, to start the calculation, and then calculated, using the compliance matrices ($Cmat$) of the parts, once the pressure distribution (P) is determined.

$$d = Cmat * P \quad (1)$$

In the previous version, only the dynamic deformations of the piston was considered. Introducing now the dynamic deformation of the liner, in theory, we should distinguish between piston and liner deformations. However, since the deformations are eventually only used to define the clearance volume (h) for the pressure calculation, it is possible to sum up the piston and liner deformation and consider it as a unique variable.

$$d_{tot} = d_{piston} + d_{liner} \quad (2)$$

$$h = f(lateral\, motion, tilt\, angle, d_{tot}) \quad (3)$$

Once the pressure distribution is calculated, all the deformations are determined by virtue of a linear relation, therefore we can simply and directly calculate the total deformation, using the compliance matrices of the two parts, as expressed in following equations.

$$d_{piston} = Cmat_{piston} * P \quad (4)$$

$$d_{liner} = Cmat_{liner} * P \quad (5)$$

$$d_{tot} = d_{piston} + d_{liner} = \left(Cmat_{piston} + Cmat_{liner}\right) * P \quad (6)$$

In summary, the deformation term, that in the old model only accounted for piston's deformation, it now takes into account the deformations of both piston and liner. This does not create problems in the solving mathematical scheme, because the number of variables is not changed and the relation between pressure distribution and deformations is always linear. In the end, the only thing changed is that the compliance matrix used is the sum of piston and liner compliance matrix.

$$Cmat_{tot} = Cmat_{piston} + Cma_{liner} \quad (7)$$

Note that the Jacobean of the system of equations does not need to be changed, because the number of variables and equations, which define the relations among these variables, have not changed.

Lastly, it needs to be mentioned that for each time step in the calculation only the compliance on the liner in the area covered by the piston is considered. Therefore, interpolation is used to achieve the liner's compliance that matches the meshing of the piston's compliance.

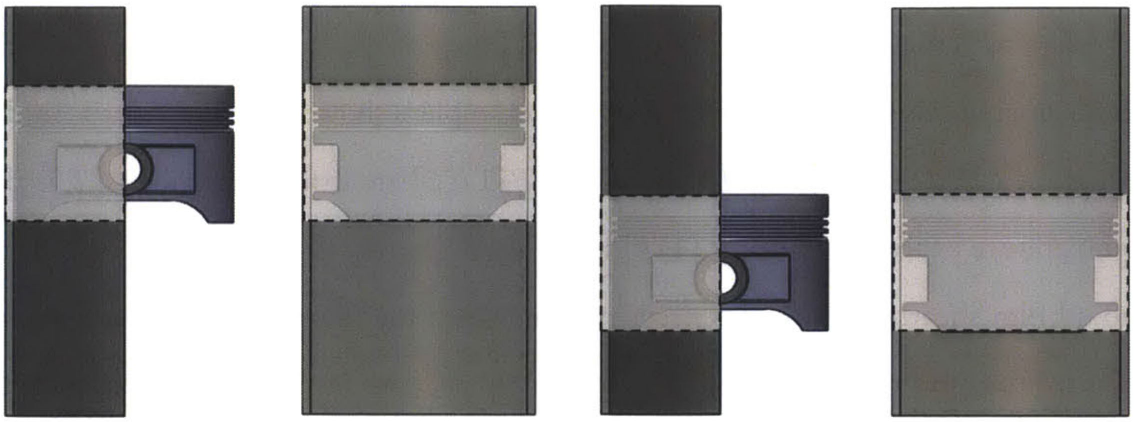

Figure 2.14– Portion of liner compliance isolated for thrust side calculation, at two different crank angles

Once the calculation is finished and the dynamical stresses acting on the liner have been determined, one can easily recover its total deformation using its complete compliance matrix.

2.4 Shear-thinning and temperature effect on viscosity

The viscosity of the oil is a really important for the skirt's lubrication. As discussed previously, viscosity is affected by temperature and shear rate. The relation used to describe the viscosity, in function of temperature and shear rate, is a combination of the Vogel and Cross equations. Shell, which is a member of our consortium, used the Vogel and Cross equation to model viscosity across a broad shear rate ranges [11]. The equation is formulated as follow:

$$\mu(\gamma, T) = \kappa \exp\left(\frac{\theta_1}{\theta_2 + T}\right) \cdot \left(\frac{\mu_\infty}{\mu_0} + \frac{1 - \frac{\mu_\infty}{\mu_0}}{1 + \left|\frac{\gamma}{10^{A+BT}}\right|}\right) \quad (8)$$

Equation (8) is usually obtained fitting experimental measurements of viscosity with the Vogel and Cross equations. Equation (8) is usually obtained fitting experimental measurements of viscosity. An example is showed in Figure 2.15. In the equation κ $[Pa \cdot s]$, $\vartheta_1[°C]$, $\vartheta_2[°C]$, A and $B[1/°C]$ are fitting parameters; T is the temperature expressed in $°C$; γ $[1/s]$ is the shear rate; μ_0 is the viscosity value with no oil film shearing, μ_∞ is the viscosity value when the shear rate has its maximum effect. From the viscosity results of the example oil, it is possible to notice that both temperature and shear-thinning effect can cause the viscosity to drop consistently. This behavior, however, is different from oil to oil, depending on base oil and viscosity modifier.

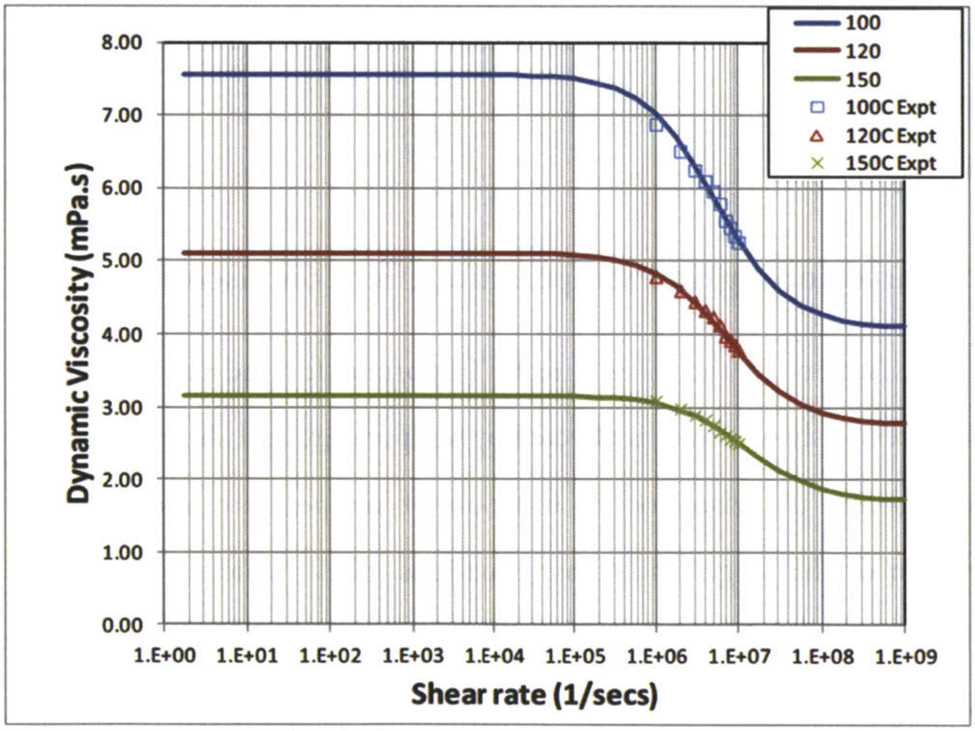

Figure 2.15 – Example of oil viscosity measurements and data fitting results.

As discussed in the previous section, it is always necessary to analyze the solving mathematical scheme of the model, when introducing new variables or relations into it. In this case the parts that need to be discussed are the hydrodynamics solver and the Jacobean of the system of equations.

The temperature used in the model, in order to calculate the viscosity, is the average temperature of piston and liner at every specific crank angle. This temperature is given as an input data, therefore for every calculation step it is fixed and does not represent a problem for the convergence of the model. The shear rate dependence, however, can affect the solving scheme.

Due to the motion of the piston, the oil film can shear in consequence of Couette or Poiseuille flow [10]. The contribution of the Couette flow to the shear rate can be easily determined, since it only depends on the velocity of the piston, which can be univocally calculated. On the other hand, the contribution of the Poiseuille flow cannot be rapidly determined, because it depends on the pressure distribution, which itself is affected by the viscosity. In other words, in order to calculate the viscosity accurately, the pressure distribution needs to be known, and vice versa, in order to calculate the pressure, the viscosity has to be determined.

The way to solve this problem is to slightly modify the hydrodynamic solver. Basically, in order to start the solver, the viscosity is first calculated considering only temperature and Couette flow. Once the viscosity is determined, a first approximation for the pressure is found and the viscosity is updated, considering also the Poiseuille flow. This process is repeated until the pressure is consistent with the viscosity.

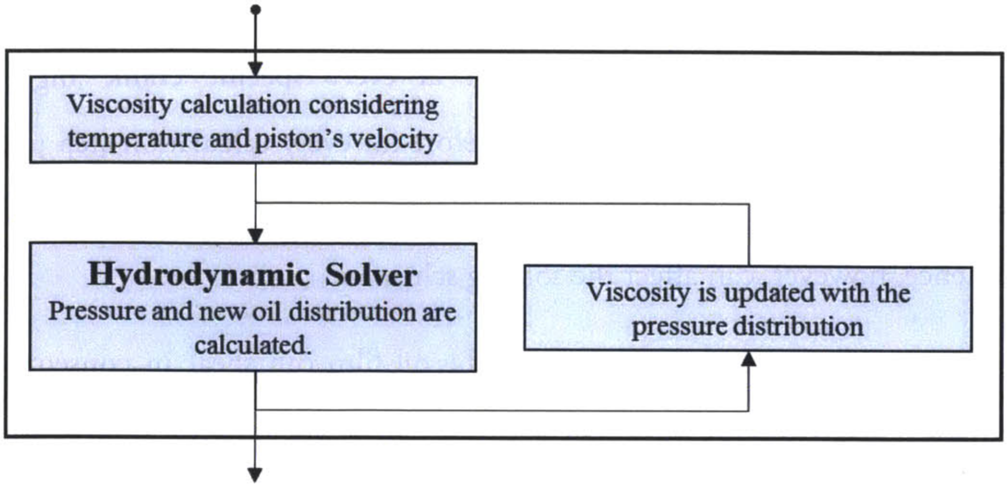
Viscosity calculation considering temperature and piston's velocity
Hydrodynamic Solver
Pressure and new oil distribution are calculated.
Viscosity is updated with the pressure distribution

Figure 2.16 – Modification to the hydrodynamic solver

Note that the shear rate consequent from the Poiseuille flow changes along the film thickness direction. In the model the average of the absolute value of the shear rate is used, as an approximation.

The other part that needs to be carefully analyzed is the Jacobean of the system of equations. In general given a specific set of equations and variables, the Jacobean is defined as follows.

$$System\ of\ equations: \begin{bmatrix} f_1 \\ f_2 \\ \cdot \\ \cdot \\ f_n \end{bmatrix} \cdot \begin{bmatrix} x_1 \\ x_2 \\ \cdot \\ \cdot \\ x_n \end{bmatrix} = \begin{bmatrix} b_1 \\ b_2 \\ \cdot \\ \cdot \\ b_n \end{bmatrix} \quad (9)$$

$$Jacobean: \begin{bmatrix} \frac{\partial f_1}{\partial x_1} & \cdots & \frac{\partial f_1}{\partial x_n} \\ \vdots & \ddots & \vdots \\ \frac{\partial f_n}{\partial x_1} & \cdots & \frac{\partial f_n}{\partial x_n} \end{bmatrix} \quad (10)$$

By introducing the relation for the viscosity, the number of equations and variables of the system have increased. This might affect specific parts of the Jacobean that includes the viscosity in the calculation, which is no longer kept constant. Every equation affected by this change has been analyzed.

The first equation that needs to be discussed is the torque balance equation on the piston. In this equation, the term that is affected by the viscosity is the torque applied on the piston caused by shear stresses. This term, called T_τ, is proportional to shear stress τ, skirt area A and piston radius r.

$$T_\tau = \tau A r \quad (11)$$

In the Jacobean, the term $\frac{\partial T_\tau}{\partial h}$, where h is the clearance volume, is calculated. The only term depending on h is the shear stress, which is expressed as:

$$\tau = \mu \cdot \gamma \quad (12)$$

Where γ is the shear rate. In the existing version of the model, keeping the viscosity constant, the only term included was the shear stress term, $\mu \frac{\partial \gamma}{\partial h}$. Now, in principle, we should also consider the viscosity term, $\frac{\partial \mu}{\partial h} \gamma$.

$$\frac{\partial \tau}{\partial h} = \gamma \frac{\partial \mu}{\partial h} + \mu \frac{\partial \gamma}{\partial h} \quad (13)$$

Before changing the Jacobean, however, it is necessary to check if the viscosity term is dimensionally important when compared to the shear stress term. To do so, the term $\gamma \frac{\partial \mu}{\partial h}$ has to be estimated using the viscosity equation (8).

$$\gamma \frac{\partial \mu}{\partial h} = \gamma \, \kappa \exp\left(\frac{\theta_1}{\theta_2 + T}\right) \cdot \left(\frac{-1 + \frac{\mu_\infty}{\mu_0}}{\left(1 + \left|\frac{\gamma}{10^{A+BT}}\right|\right)^2} \right) \left(\frac{1}{10^{A+BT}}\right) \frac{\partial \gamma}{\partial h} \quad (14)$$

Therefore:

$$\gamma\frac{\partial\mu}{\partial h}\Big/\mu\frac{\partial\gamma}{\partial h}=\frac{\gamma\,\kappa\exp\left(\frac{\theta_1}{\theta_2+T}\right)\cdot\left(\frac{-1+\frac{\mu_\infty}{\mu_0}}{\left(1+\left|\frac{\gamma}{10^{A+BT}}\right|\right)^2}\right)\left(\frac{1}{10^{A+BT}}\right)\frac{\partial\gamma}{\partial h}}{\kappa\exp\left(\frac{\theta_1}{\theta_2+T}\right)\cdot\left(\frac{\mu_\infty}{\mu_0}+\frac{1-\frac{\mu_\infty}{\mu_0}}{1+\left|\frac{\gamma}{10^{A+BT}}\right|}\right)\frac{\partial\gamma}{\partial h}}$$

$$=\frac{\gamma\left(\frac{-1+\frac{\mu_\infty}{\mu_0}}{\left(1+\left|\frac{\gamma}{10^{A+BT}}\right|\right)^2}\right)\left(\frac{1}{10^{A+BT}}\right)}{\left(\frac{\mu_\infty}{\mu_0}+\frac{1-\frac{\mu_\infty}{\mu_0}}{1+\left|\frac{\gamma}{10^{A+BT}}\right|}\right)} \qquad (15)$$

Using the data from several oils and considering a shear rate ranging from 10^5 to 10^7 $1/s$, it is possible to get an approximation for the relative importance of the two terms. The resulting estimate ranges from 0.002, for average temperature and shear rate, to roughly 0.1, for critical condition, namely maximum shear rate and high temperatures. This result shows that the shear rate term, $\mu\frac{\partial\gamma}{\partial h}$, has usually a much stronger influence in the Jacobean than the viscosity term. It is true that for critical conditions, the viscosity term increases its importance, but it is not a dominant behavior. The torque balance equation, in fact, has not been modified to introduce the viscosity influence and the convergence of the model, tested in several applications, has resulted not compromised.

Another equation that needs to be discussed is the oil transport equation. This equation is used to calculate the oil flow, and eventually the oil distribution, over the piston's skirt. It has been derived using the averaged Reynolds equation, applied to every point in the calculation domain [4], and describes the oil flow from point to point in function of the pressure gradient. Note that the oil flow due to Coette flow is also calculated, but it is not dependent on viscosity, therefore it is not considered in this discussion.

The equation that follows describes the oil flow rate q, along an arbitrary direction x, in m^3/s, in function of the oil film thickness h_{film}. Note that in the model, for every point in the calculation domain it is associated a cell, for which pressure and oil film thickness are defined. In the equation, the cell's dimensions are defined as Δx and Δz, whereas Δp is the pressure difference across two cells.

$$q_x = -\frac{h_{film}^3}{12\,\mu}\frac{\Delta p}{\Delta x} \cdot \Delta z \quad (16)$$

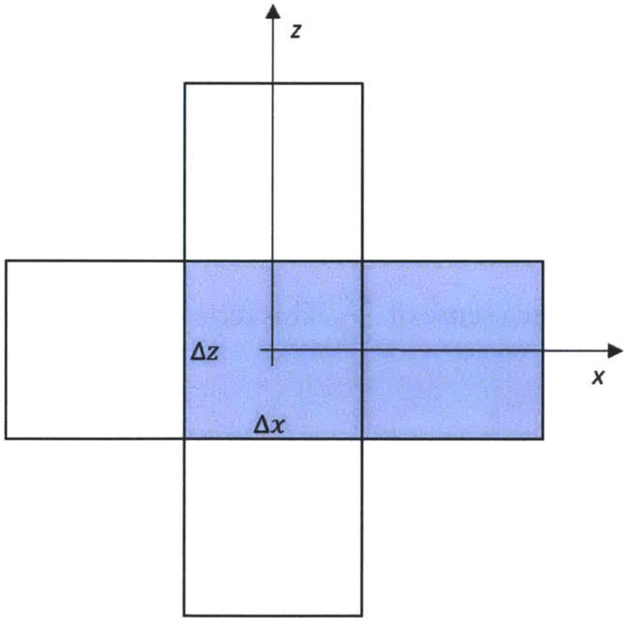

Figure 2.17 – Cells definition in the calculation domain

The oil flow depends, again, on the clearance volume, since the pressure is determined in the hydrodynamic solver. The equation used in the Jacobean is, therefore, the derivate of q_i with respect to h.

$$\frac{\partial q_x}{\partial h} = -\frac{\Delta p}{\Delta x} \cdot \Delta z \cdot \left(3 \frac{h^2}{12\,\mu} - \frac{h^3}{12\,\mu^2} \frac{\partial \mu}{\partial h}\right) \quad (17)$$

As we have seen for the torque balance equation, the viscosity has to be considered here too, but it is again necessary to check if its influence is dimensionally comparable with the term $3\frac{h^2}{12\,\mu}$, which is considered in the existing model.

$$\frac{\frac{h}{\mu}\frac{\partial \mu}{\partial h}}{3} = \frac{\frac{\partial \mu}{\partial h}}{\frac{3\mu}{h}} = \frac{\left(\frac{-1+\frac{\mu_\infty}{\mu_0}}{\left(1+\left|\frac{\gamma}{10^{A+BT}}\right|\right)^2}\right) \cdot \left(\frac{1}{10^{A+BT}}\right) \frac{\partial \gamma}{\partial h}}{3\left(\frac{\mu_\infty}{\mu_0} + \frac{1-\frac{\mu_\infty}{\mu_0}}{1+\left|\frac{\gamma}{10^{A+BT}}\right|}\right) \cdot \frac{1}{h}} \quad (18)$$

All quantities can be estimated considering several oils and clearance values, however, it is harder to get a sense of $\frac{\partial \gamma}{\partial h}$. This term can be affected from both Couette and Poiseuille flow.

$$\frac{\partial \gamma}{\partial h} = \left(\frac{\partial \gamma}{\partial h}\right)_{Couette} + \left(\frac{\partial \gamma}{\partial h}\right)_{Poiseuille} \quad (19)$$

The two terms scale differently with the clearance volume.

$$\left(\frac{\partial \gamma}{\partial h}\right)_{Couette} \propto \frac{v_{piston}}{h^2} \quad (20)$$

$$\left(\frac{\partial \gamma}{\partial h}\right)_{Poiseuille} \propto \mu h \frac{\partial p}{\partial x} \quad (21)$$

However, the Couette contribution, due to the $1/h^2$ term, has a much stronger influence than the Poiseuille contribution, for every given value of viscosity or pressure gradient. Therefore, for the purpose of estimating the viscosity importance in the oil flow equation, we can only consider the Couette term for $\left(\frac{\partial\gamma}{\partial h}\right)$. Equation (18) can be re-written as:

$$\frac{\frac{h}{\mu}\frac{\partial\mu}{\partial h}}{3}=\frac{\frac{\partial\mu}{\partial h}}{\frac{3\mu}{h}}\cong\frac{\left(\frac{-1+\frac{\mu_\infty}{\mu_0}}{\left(1+\left|\frac{\gamma}{10^{A+BT}}\right|\right)^2}\right)\cdot\left(\frac{1}{10^{A+BT}}\right)\frac{v_{piston}}{h}}{3\left(\frac{\mu_\infty}{\mu_0}+\frac{1-\frac{\mu_\infty}{\mu_0}}{1+\left|\frac{\gamma}{10^{A+BT}}\right|}\right)} \qquad (22)$$

The resulting estimate of the ratio above ranges from 0.01 to 0.07, using piston average velocity up to $20\ m/s$, clearance volume between 10^{-5} and $10^{-6}\ \mu m$, and shear rate between 10^5 and $10^7\ 1/s$. Given the small influence that the viscosity would have, the corresponding oil flow equation in Jacobean, does not need to be modified.

In summary, by introducing the viscosity equation in the model, the only part that needed to be modified was the hydrodynamic solver. The Jacobean has remained the same, because the influence of viscosity is not comparable with the influence or other variables. One section in Chapter 3 will focus on the effect that temperature and shear rate have on viscosity, comparing different studies on the floating liner engine.

2.5 Arbitrary skirt domain definition

The aspect of the model that has been modified is the definition of the calculation domain. Previously the domain was assumed rectangular and identical for thrust and anti-thrust side, but this setup becomes restrictive in real application as modern piston's skirt presents a fairly irregular shape, as shown in Figure 2.18, right.

By introducing an arbitrary definition of skirt, luckily, it is not necessary to make important modifications to the mathematical solving scheme, as the physics of the problem remains the same. However, since the domain is not simply rectangular anymore, the way the input data, which defines the piston, need to be processed has become more complicated.

Previously, even if the skirt had not a perfectly rectangular shape, the user had to define a rectangular region within it, in order to set up the domain. Since in the current model the domain can have an arbitrary shape, this process need to be automated, in fact, a border detection algorithm has been formulated and included.

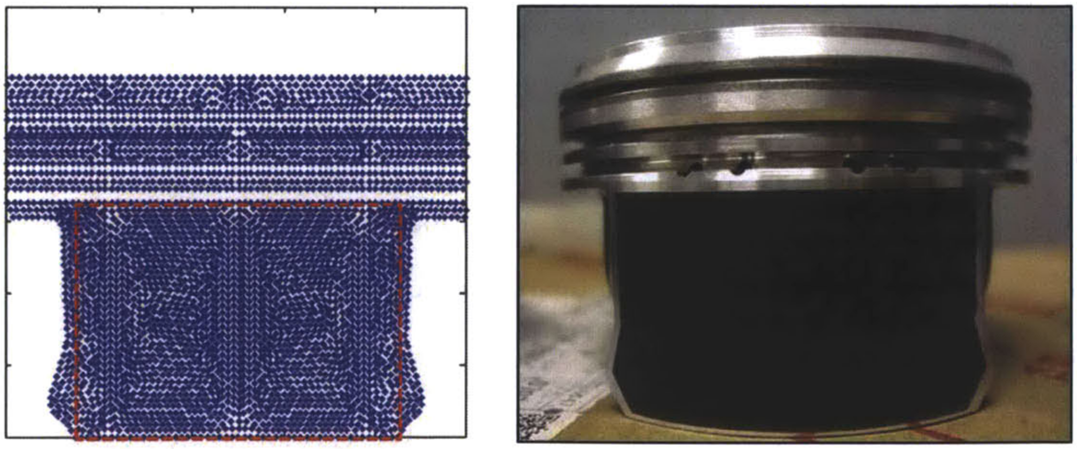

Figure 2.18 – Skirt input data and rectangular domain definition (left)
Modern piston's skirt – thrust side (right)

The theory beyond border detection algorithm is quite complicated, especially when the border is concave. In literature, it is known that the best way to detect arbitrary borders is to use the Delaunay triangulation method [12]. This approach is, however, too complicated for our purposes, therefore a new, simpler and more intuitive algorithm has been developed.

This algorithm relies on the Matlab function called *convhull*, which is able to detect the border of convex figures. The only application of this function, however, does not allow to find the concave boundary, in fact, applying *convhull* to the skirt in Figure 2.19, the results would be the following, where the points in red are those detected as boundary.

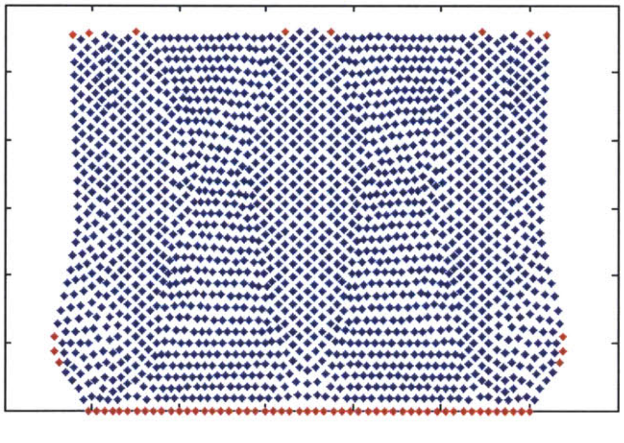

Figure 2.19 – Convex boundary detection

The use of the function, as it is, is not successful. The algorithm, however, in order to complete the process, transforms the point cloud before applying the function. The basic idea is to make the concave portions of the point cloud convex so that the *convhull* function will be able to recognize them. In the end, the goal is only to get the indices of the points on the boundary, therefore this method would work.

Qualitatively, what the transformation does is to stretch the figure along a particular axis, as shown in Figure 2.20.

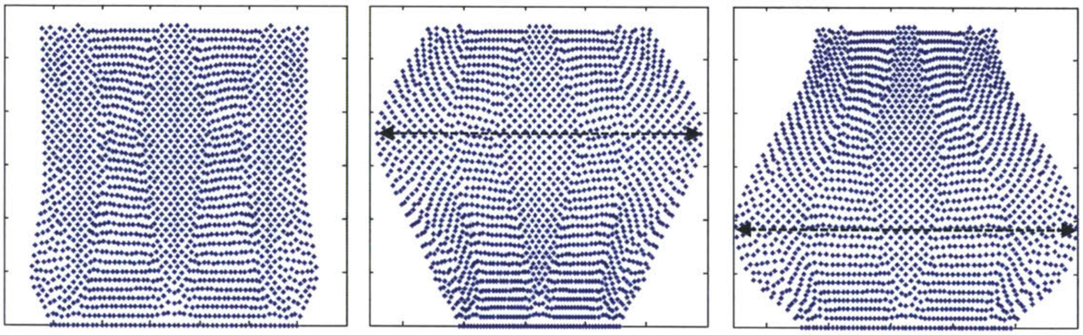

Figure 2.20 – Point cloud transformation

Mathematically the transformation is done with the following equation.

$$\Delta th = C \cdot \exp(-z^2) \cdot th \tag{23}$$

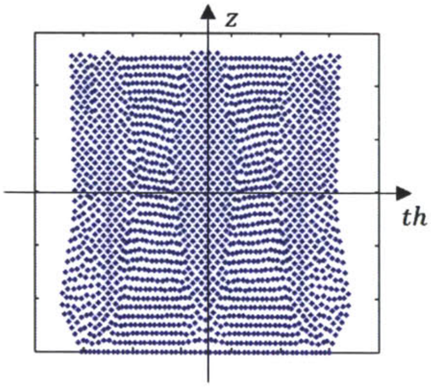

The z and th coordinate refer to the plotted axis and are used to determine the points' position. Δth is the displacement from the z axis, at which every point is subject to. The equation applies a bigger displacement to the point that are on th axis and far from the z axis.

Once the figure has been transformed, the $convhull$ function is applied. This process is repeated multiple times, changing the vertical position of the th axis and rotating both axis, in order to recognize all the concave regions.

This algorithm turns out to be really efficient in finding all kinds of boundary, some example are reported below. This approach can be really useful also in other kinds of problems, where it is necessary to find the boundary of densely populated point cloud, like those of the input data for this model.

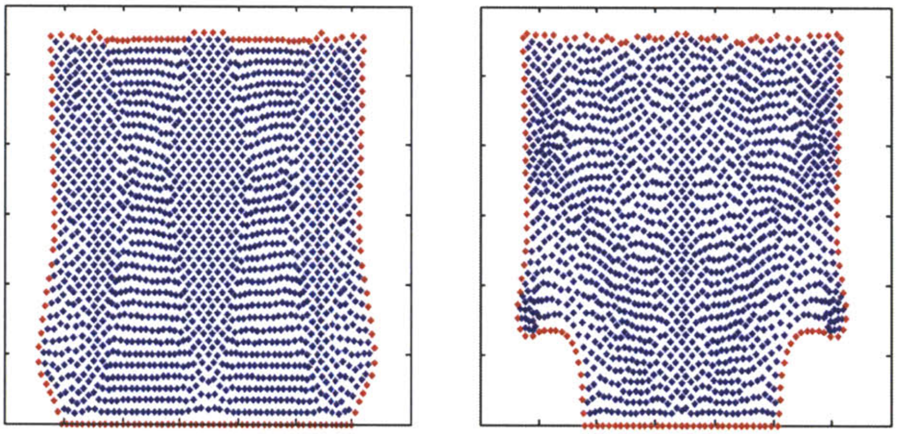

Figure 2.21 – Example of boundary calculation

Once the boundary has been detected, a rectangular grid is over imposed to the point cloud and only the cells situated inside the detected boundary are included the domain of calculation.

These are the most important and interesting changes made in the model to handle arbitrary skirt's shapes. Unfortunately, no case has been studied yet using this very latest version of the model, therefore it will be left as a future objective to check how influent the consideration of the whole skirt is in the calculations, if compared to the existing version.

Chapter 3

Comparison of model's results with experimental results

3.1 Floating liner engine set-up description

One of the experimental set-up in the Sloan Automotive Laboratory is the Floating Liner Engine [13]. The purpose of this experiment is to directly measure the friction force between piston and liner.

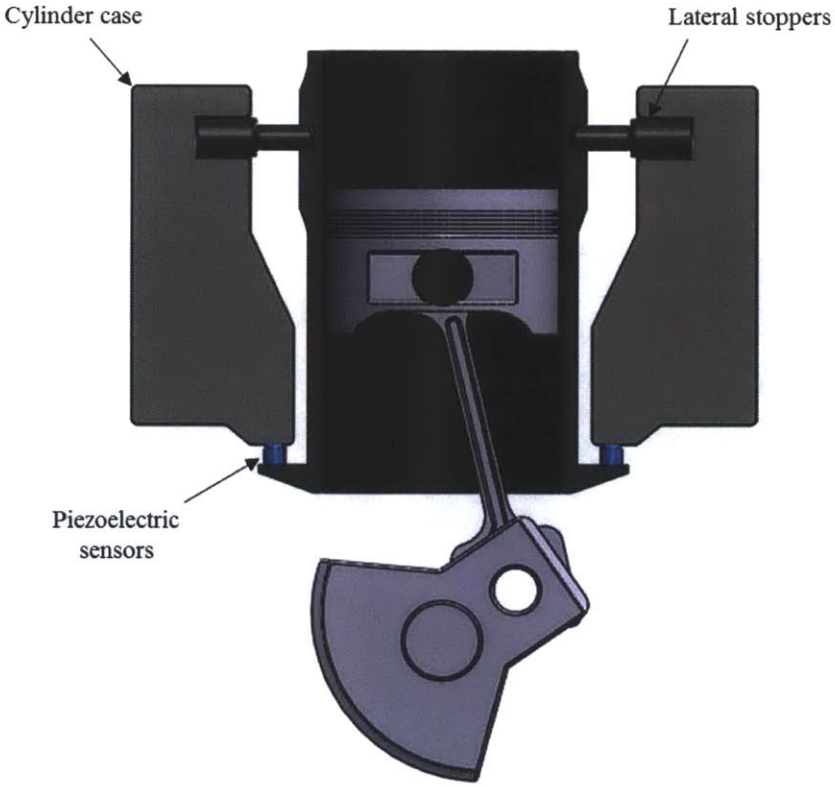
Cylinder case
Lateral stoppers
Piezoelectric sensors

Figure 3.1 – Floating Liner Engine set-up schematic

As shown in Figure 3.1, the idea is to leave the liner free to move vertically, so that the piezoelectric sensors, connected to it, would be able to measure the pressure that the liner applies on them, and achieve, in this way, the vertical force that the piston applies on the liner, namely the friction force. This measurement process, however, can be affected by the secondary motion of the piston, therefore lateral stoppers are connected to the liner to limit its horizontal motion.

Nevertheless, since the stoppers are not able to completely prevent the liner from moving or even rotating, the measurements are affected. In order to understand this behavior a few cases will be analyzed.

Starting from the ideal cases, in which the secondary motion should not affect the measurements, the sensors are supposed to give the same measurements. For example, during a down-stroke both sensors should be stretching and during an up-stroke compressing. Note that in Figure 3.2 and throughout this section, stretching is indicated with green color, compression with red color.

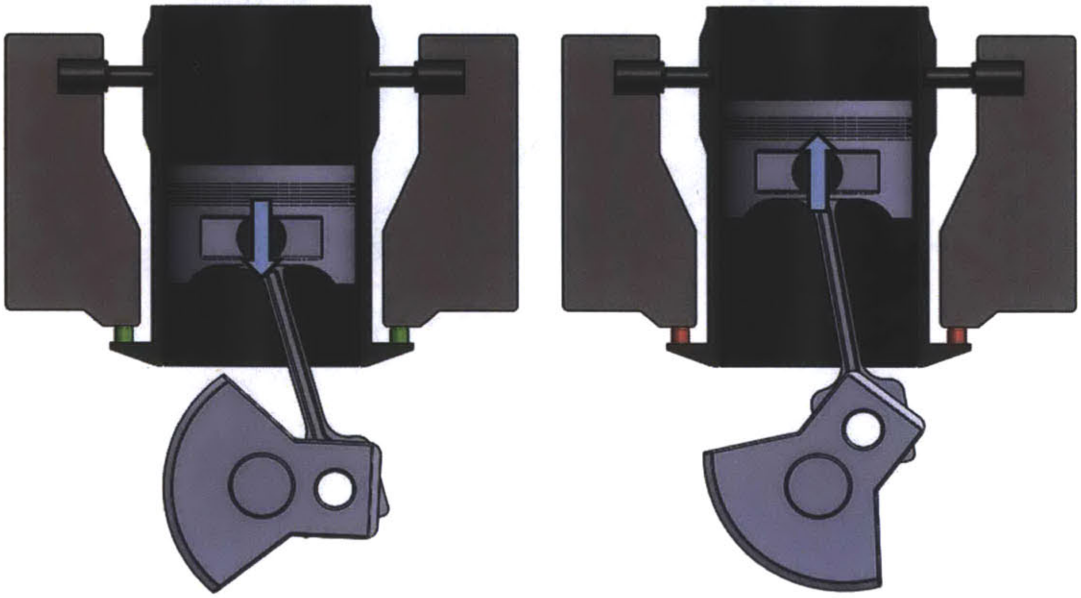

Figure 3.2 – Stretching (left) and compression (right) of piezoelectric sensors

When, however, the side force applied on the piston and, consequently, the secondary motion are significant, the sensors can measure forces of different sign. For example, during a down-stroke, if the piston is pushing toward the anti-thrust side, the side force can be strong enough to induce the liner block to rotate. This motion is not excessive, however it can be definitively captured by the sensors. In some cases it can be measured that the sensor on the anti-thrust side is stretching while the one on thrust side is compressing.

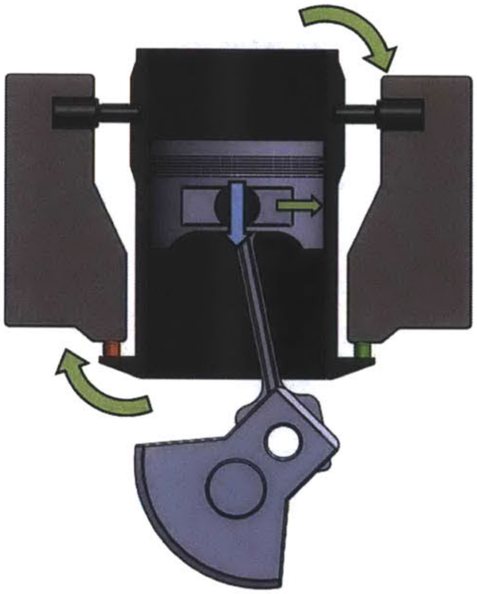

Figure 3.3 – Sensors' behavior during down-stroke, with a strong side force

Similarly, also during an up-stroke the sensors might measure opposite forces. In this case, if the piston is pushing toward thrust side, the sensor on this side can be stretching, instead of compressing, and the sensor on thrust side can be compressed even more.

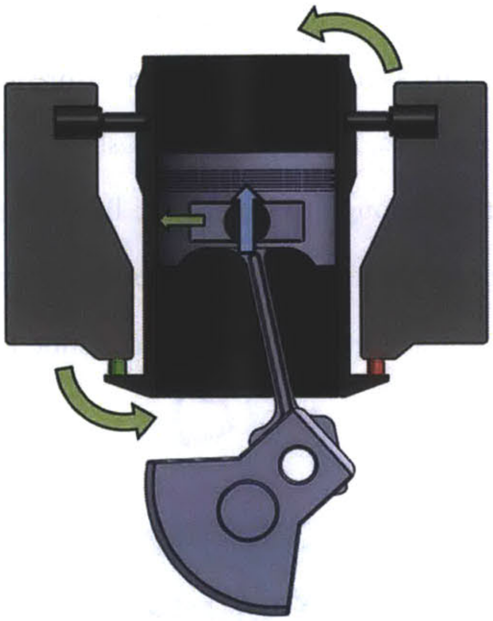

Figure 3.4 – Sensors' behavior during up-stroke, with a strong side force

Looking at actual measurements, one can realize how significant this phenomenon is.

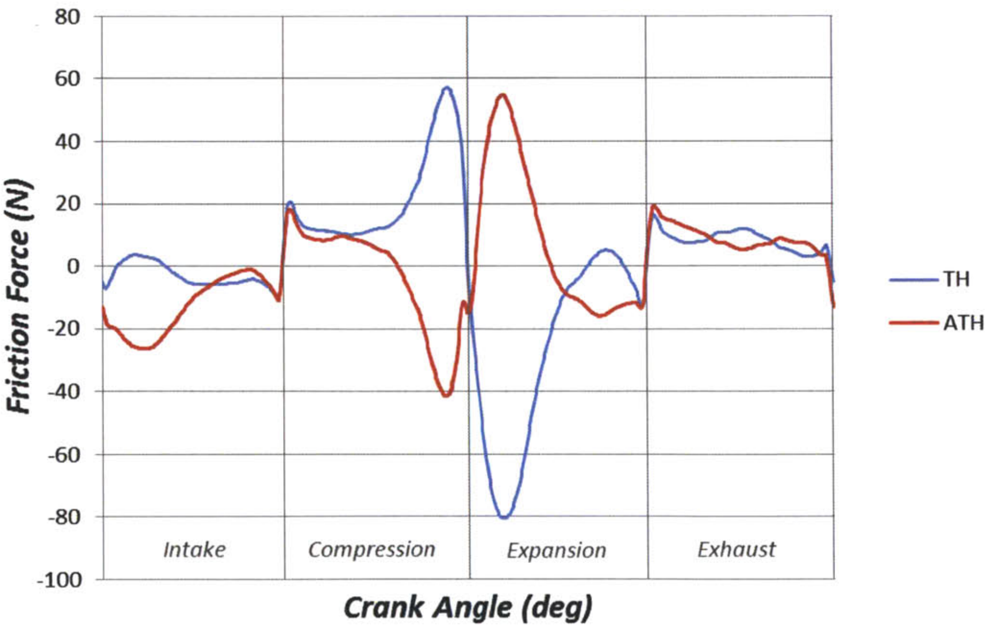

Figure 3.5 – Friction measured by the sensors on thrust and anti-thrust side

From Figure 3.5, it is possible to note that this phenomenon is particularly significant near TDC.

Certainly, this aspect needs to be taken into account when comparing measurements and calculations. In fact, since the total friction is calculated as sum of the measurements from both sensors, it will not be accurate in points, during cycle, where the measurements have opposite sign. On the other hand, however, this phenomenon can be of help in order to get an idea of the secondary motion of the piston. This last topic will be discussed in Section 3.3.

Lastly, another important aspect of the measurements obtained is their variation from cycle to cycle. Normally two main factors cause this variation: the instability of the combustion process, which gives different pressure traces every cycle, and the oil supply to the piston-liner interface, which is a chaotic phenomenon and cannot be easily predicted. Looking at example set of measurements obtained for a specific condition, the variation, at some points in the cycle, can be rather significant. In Figure 3.6 the maximum and minimum friction measured for a test run at 1000 rpm and 2 bar load are shown.

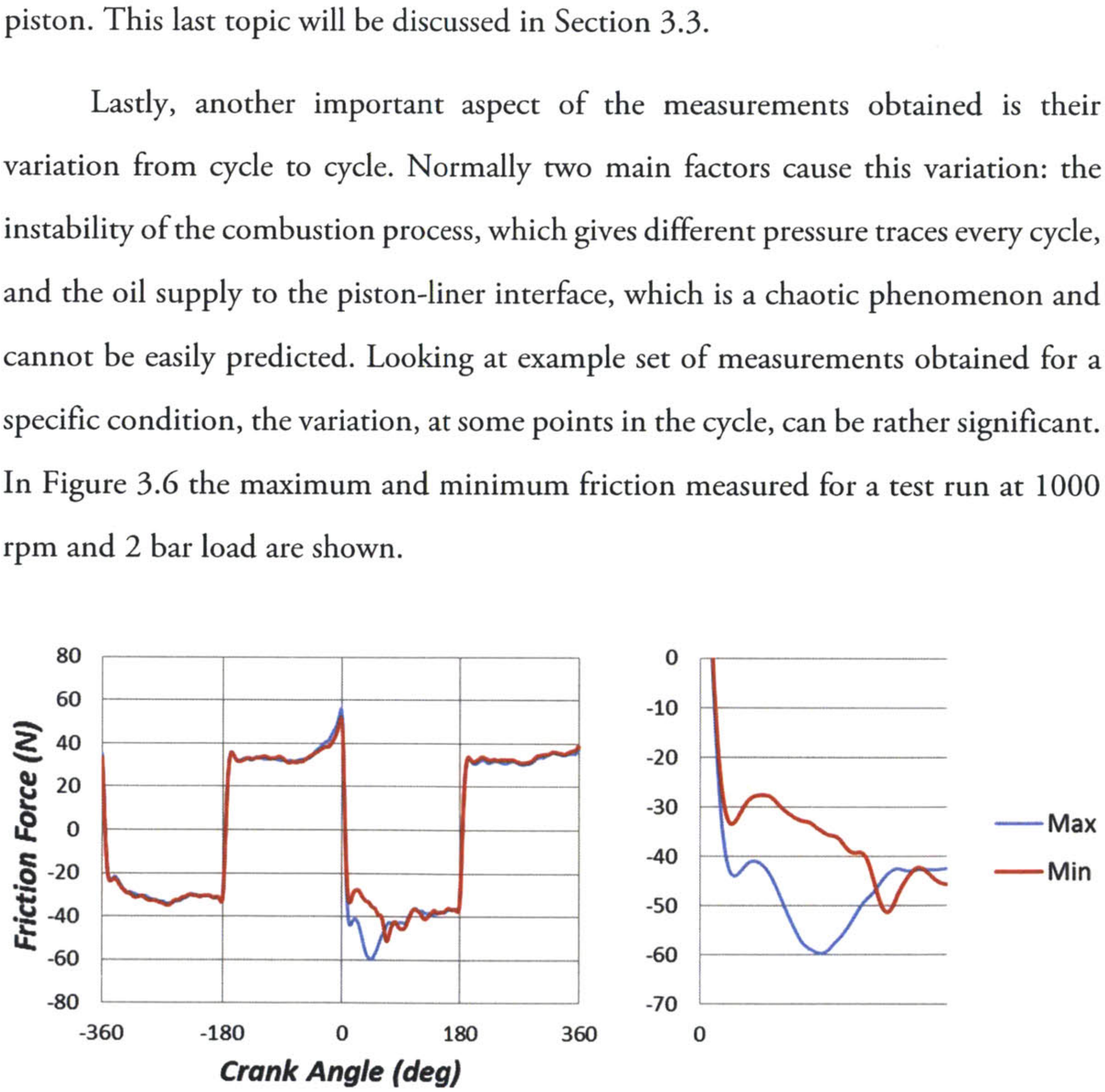

Figure 3.6 – Cycle's friction (left) and expansion stroke (right) friction variation

Given the importance of this phenomenon, it needs to be considered when comparing calculations and measurements. Even if the combustion pressure's influence on this variation can be limited, if the average pressure trace is used in the calculation, the real oil supply cannot be predicted and it can still cause differences between experiments and simulations.

In the next section measurements and calculations for specific conditions will be compared. The friction compared to the calculations' results will be the average friction experimentally measured over several hours of testing.

3.2 Friction results comparison

Similarly to every model that aims to describe a particular phenomenon in internal combustion engines, it needs to be validated comparing its results with experimental observations. This section will focus on the analysis of a few engine's operating conditions, in order to verify the accuracy of the model. Note that this study is not concluded yet, in fact more operating conditions need to be tested, in order to infer on the model's validity; nonetheless, the results obtained in this chapter are a good starting point to understand what can be improved and what can be relevant in the calculations.

Figure 3.7 summarizes the cases analyzed in this study. The engine operating conditions studied so far are only two: 1000 rpm with IMEP of 2 bar and 1000 rpm with IMEP of 4 bar. The model has been run both assuming a constant viscosity of $0.005\ Pa \cdot s$ and considering the viscosity relation, expressed by equation (8), using $HTHS2.9$ oil, for which the rate of low shear rate and high shear ratio viscosity is 0.5404. The piston' skirt has been coated with graphite, which has a boundary friction coefficient of 0.03. The oil supply to the system, as defined in Section 2.2, is assumed $25\ \mu m$ per revolution. This way to describe the oil supply may not be accurate, and the influence of this parameter will be a subject for future investigation. Also, in order to give an idea of the engine tested, same geometrical parameters are reported in Figure 3.8.

Speed	$1000\ rpm$	
Load	$2\ bar\ IMEP$	$4\ bar\ IMEP$
Viscosity	$\mu = 5mPa$ constant	*HTHS2.9 oil*
Boundary friction coefficient	0.03	
Oil supply	25 μm every revolution	

Figure 3.7 – Cases studied and influent simulation's parameters

Nominal Bore	82.510 mm
Piston Diameter	82.455mm
Coated Material Thickness	15 μm in radius
Connecting Rod Length	144mm
Crank Shaft Radius	46.4mm

Figure 3.8 – Engine's data

The first group of results presented are friction calculations obtained at 1000rpm with an IMEP of 2 bar, assuming constant viscosity of $0.005\ Pa \cdot s$, compared with friction measurements. Note that the calculations does not include the ring pack friction, as the model only evaluates the hydrodynamic friction and possible contact friction of skirt or lands. The ring pack model is itself a complicated system to describe and other students in our research group are working on it. When looking at the comparisons, therefore, we need to keep in mind that the friction from the model is supposed to be smaller than the friction measured.

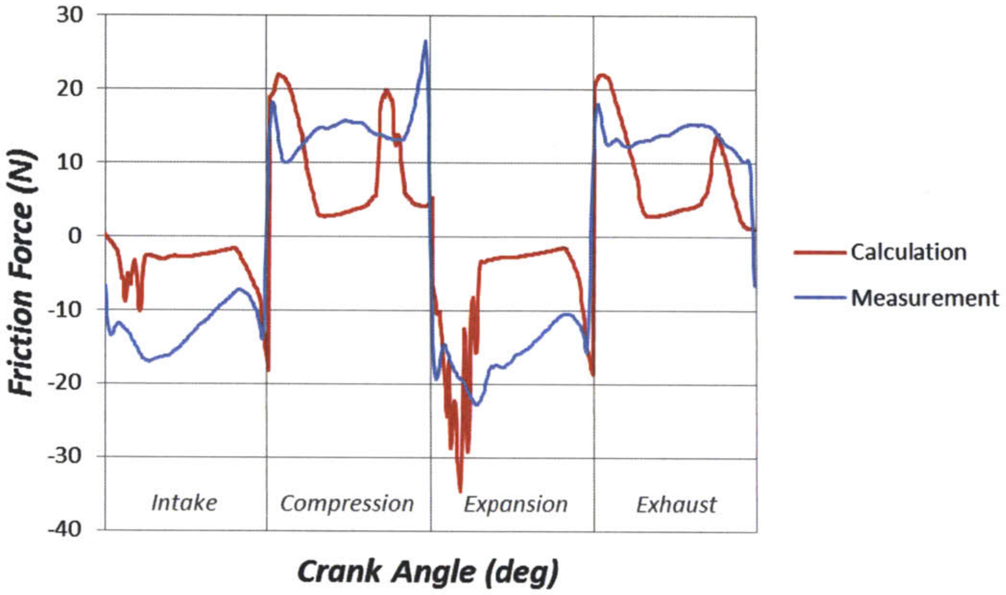

Figure 3.9 – 1000rpm - 2bar IMEP - constant viscosity
Boundary friction coefficient 0.03

From Figure 3.9, it is possible to see that in some portions of the cycle, the friction's magnitude calculated is bigger than the measurements, and since the ring friction, as explained, is not included in the calculations, this result is not satisfactory. Looking at the friction's magnitude associated with hydrodynamics and solid to solid contact (Figure 3.10), the latter results to be much more significant, therefore it is necessary to understand what causes this behavior.

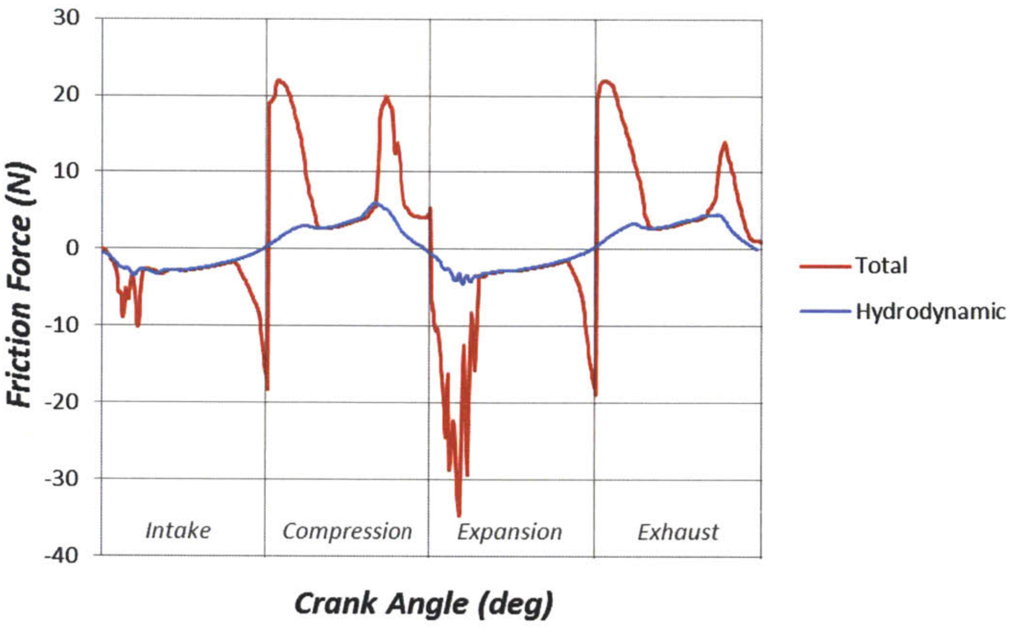

Figure 3.10 – Comparison between total and hydrodynamic friction

In general, there are several components that can affect the contact friction: boundary friction coefficient, viscosity, components' deformations and contact model used. The first one linearly influences the contact friction calculated, but its value only depends on the coating material, and it has been determined. Viscosity affects wear, hence the contact friction in the system, and will be analyzed. The piston and liner's deformations affect the geometry of the system and consequently the secondary motion, which might cause excessive contact. The specific input data for the deformations are unfortunately not easy to obtain, in fact, the liner cold and hot deformation used in the model are only approximated. Furthermore, the dynamic deformation of this component is not considered, because the compliance matrices are not available. The dynamic deformations, in particular, represent a meaningful component that needs to be taken into account in future calculations, because if the liner is assumed rigid the contact friction would tend to increase. Lastly, the solid to solid contact model is certainly something that influences the contact friction calculation and can be analyzed and improved, but it will not be a focus in this thesis.

After discussing the major components that influences the contact friction, the next study analyzes the temperature and shear-thinning effect on viscosity. The results for friction are presented as follow.

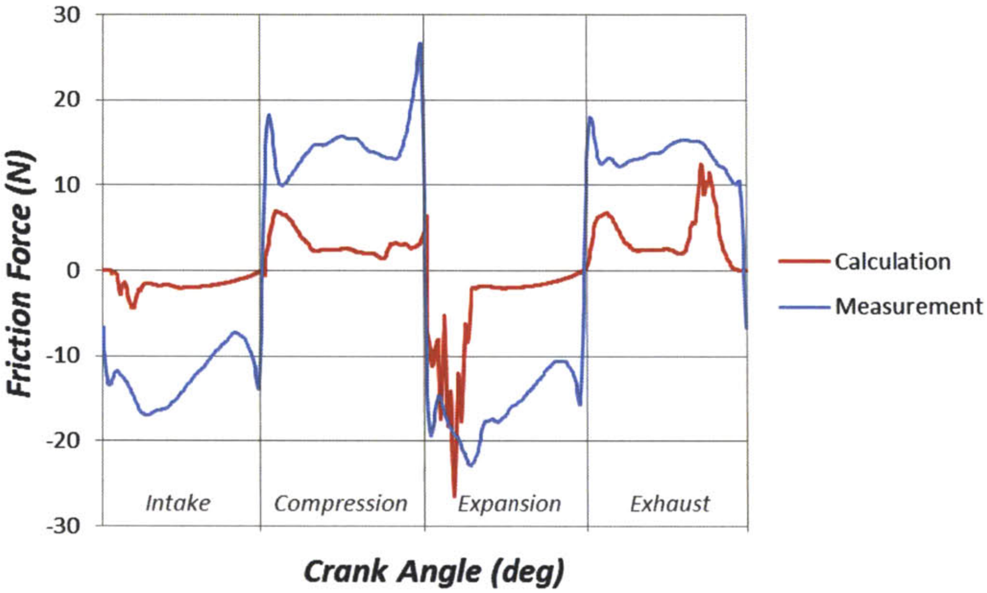

Figure 3.11 – 1000rpm - 2bar IMEP – HTHS 2.9 oil
Boundary friction coefficient 0.03

The first thing that one can note is that the contact friction for this calculation, since the hydrodynamic friction does not change significantly, it is much smaller than the corresponding case with constant viscosity. This is mainly due to the different values that the viscosity assumes during the cycle.

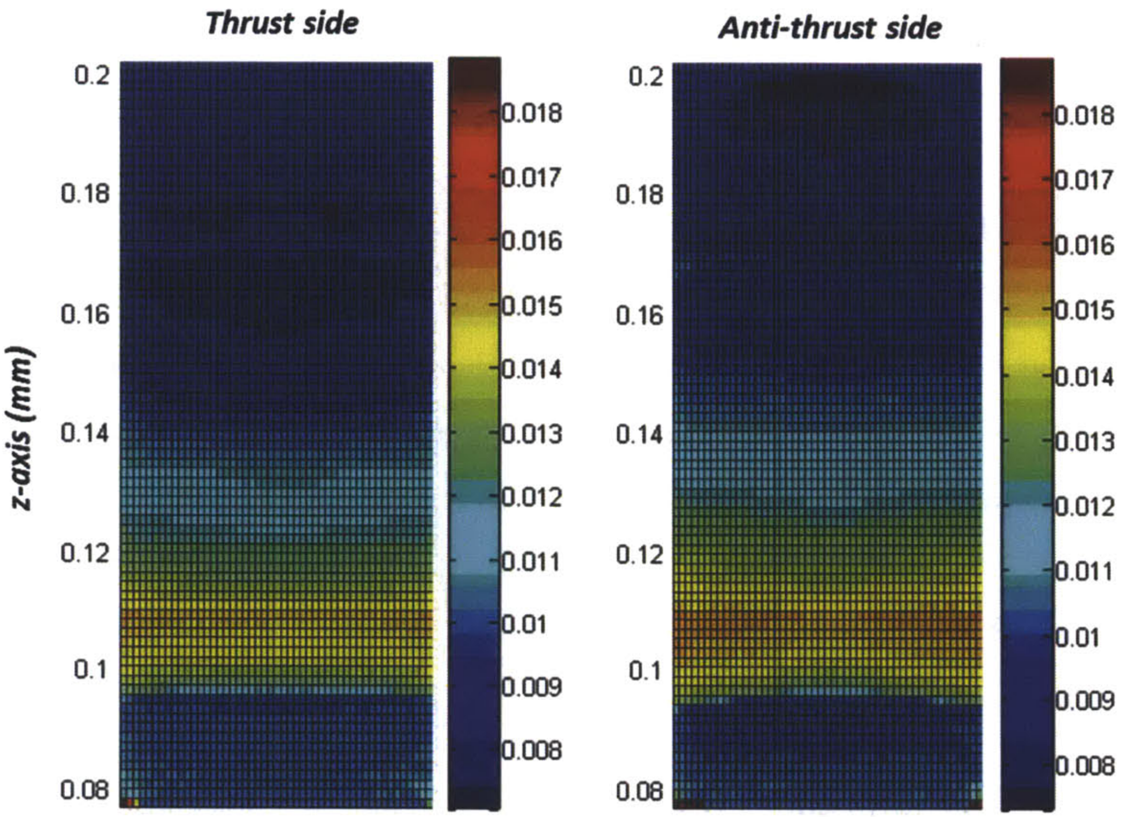

Figure 3.12 – Average viscosity value in $Pa \cdot s$ *during expansion stroke as seen on the liner*

Looking at Figure 3.12, which shows the average value of viscosity during an expansion stroke as seen on the liner, we can see that overall the viscosity has higher values than $5\ mPa \cdot s$, assumed as contact viscosity in the first calculations. Especially near BDC, where the temperature is roughly 95°C and shear-thinning effect is not excessively dominant, the viscosity ranges roughly between 0.01 and $0.016\ Pa \cdot s$. In general, higher values of viscosity lead to less solid to solid contact, which is the main difference between the two calculations presented.

Unfortunately, the only thing that it is possible to check from the results presented so far is that the calculated friction is following the right trend and its magnitude is smaller than the total friction measured. As noted previously, the model does not include the ring pack friction, therefore this represents a limitation for such study. Nonetheless, other students in our research group are working to build models to describe the ring pack [14, 26]. Yang Liu, whose work is currently focused on rings' friction calculation, has provided the rings' friction results for the running condition here studied. These results can allow to calculate the hypothetical piston's friction by subtracting the rings' friction calculated to the total friction measured and compare it with the model's calculation. Note, however, that this is approach, alone, cannot validate the model, it is only meant to give a better understanding of the model's result.

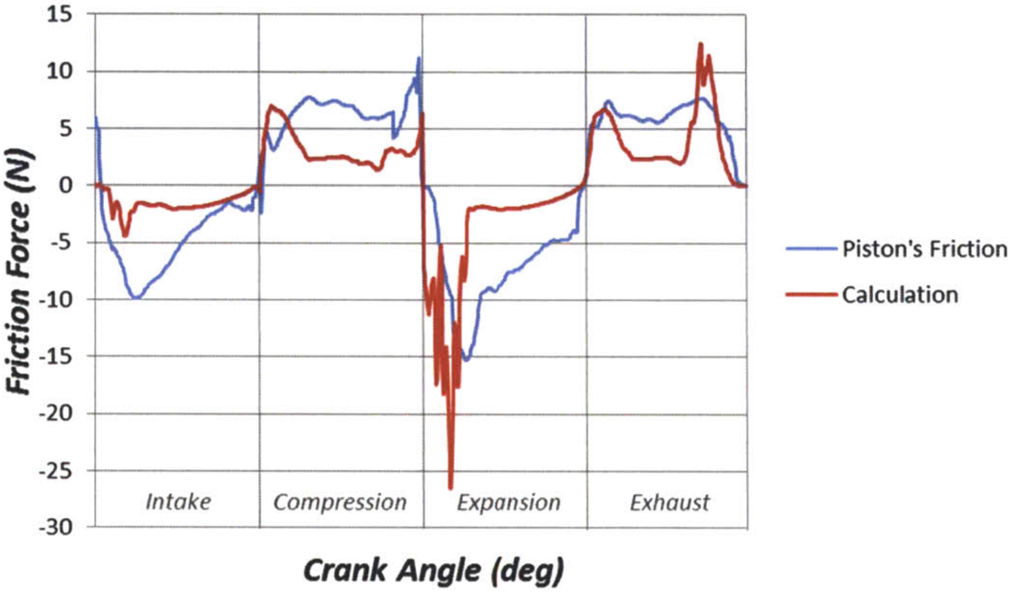

Figure 3.13 – Comparison between piston's friction calculated with the model and estimated with measurements and ring's friction calculation

Figure 3.13 shows the comparison between the calculated friction, already presented in Figure 3.9, and the hypothetical piston's friction estimated with measurements and rings' friction calculation. As we can see, in general the calculations have a good prediction of friction near TDC and BDC, however during mid-stroke we can have errors up to 10 N.

The last results presented focus on the second running condition tested: 1000 rpm, 4 bar IMEP. As follow, Figure 3.14 shows the comparison between calculation and total friction measured, Figure 3.15 the comparison between calculation and estimated piston's friction, obtained again subtracting the calculated rings' friction to the total friction measured. For brevity only the calculation done considering temperature and shear-thinning effect on viscosity are presented.

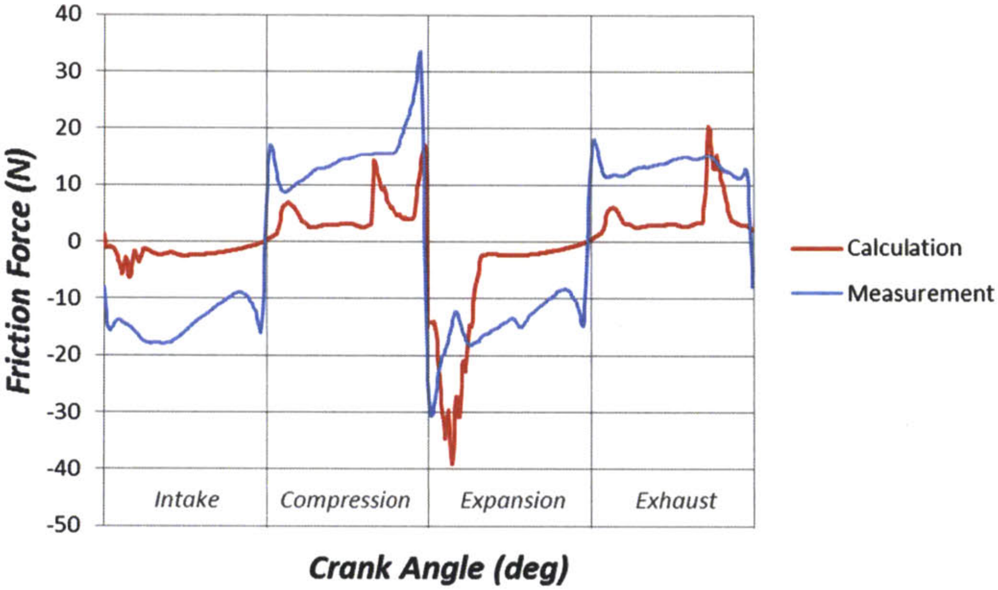

Figure 3.14 – 1000rpm - 4bar IMEP – HTHS 2.9 oil
Boundary friction coefficient 0.03

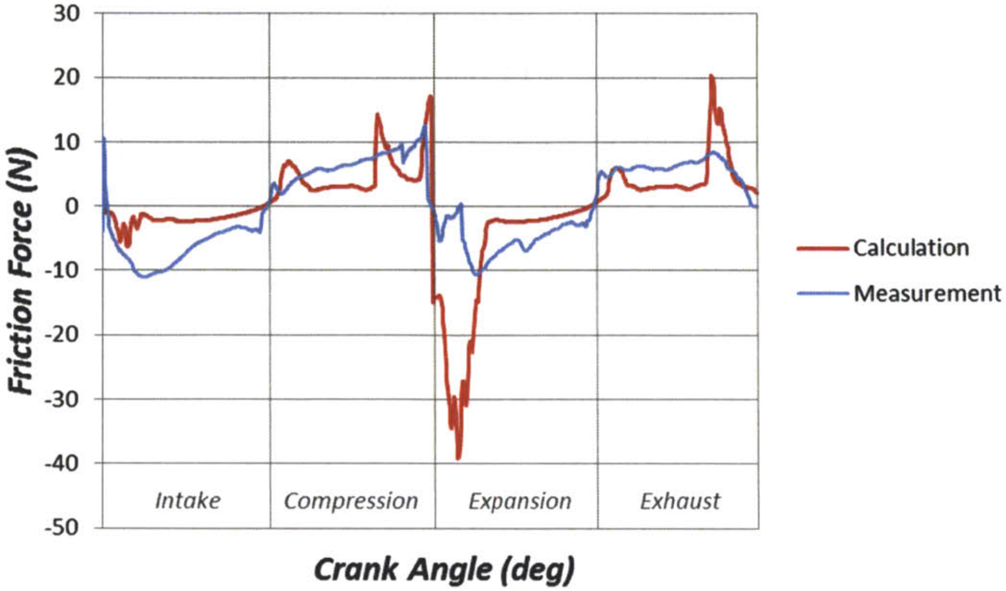

Figure 3.15 – Comparison between piston's friction calculated with the model and estimated with measurements and ring's friction calculation

The plots above shows a slightly different behavior of the calculations in respect to the previous running condition. Here the error during mid-stroke is generally smaller and we still have a good match at TDC and BDC during intake and compression stroke, however the friction at the beginning of the expansion stroke and at the end of the exhaust stroke is too high compared with the estimate.

Drawing some conclusions, this study has not been able to access the validity of the model, since more cases need to be studied. The estimated piston's friction, achieved using the ring friction's calculation, shows a good match, however this analysis is only illustrative and cannot be considered for a convincing validation. On the other hand, the study has shown the importance of considering the temperature and shear-thinning effect on viscosity in the calculation, and has brought attention on the prediction of contact friction, which causes the most important discrepancies with measurements. Furthermore, it needs to be noted that it was not possible to build a complete model of the system, because some information were not obtainable: for example, the data for the liner dynamic deformation were not available and the liner is considered rigid, its thermal deformation is only approximated, and also the oil supply to the system, which is influent in the measurements, cannot be easily determined. Other uncertainties are also related to the measurement system, which have been described in the previous section. The next step in this study would be to complete the definition of the model, gathering all the missing information, and simulate other running condition. In particular, it is necessary to test different oil supply, in order to study its influence on the results, and more importantly different pistons, in order to highlight the friction's differences related to this component. This would be the best way to understand if any part in the model need to be improved.

3.3 Secondary motion trend estimation

As introduced in Section 3.1, the secondary motion can affect the measurements that the piezoelectric sensors give. This certainly affects negatively the accuracy of the results, nonetheless, this defect can constructively be used to achieve an estimation for the trend of piston's secondary motion and compare it with the model's results. It is important, however, to note that it is reasonable to use this approach only in points during the cycle where the sensors give signals of opposite sign, because only in these points the secondary motion appreciably affects the measurements. From Figure 3.5, it is possible to see that the strokes that are mostly affected by this phenomenon are the intake, compression and expansion stroke, therefore these will be analyzed.

The approach used is to take the difference of the measurements given by the sensors in N and compare it with the lateral motion calculated with the model. Note that the purpose is not to compare their values but to compare their trend. As stated at the beginning of this section, this study is just meant to give a sense of secondary motion, it is not supposed to validate the model results. Only one case is analyzed here that is the running condition at 1000 rpm and 2 bar IMEP, the plots below summarize the results.

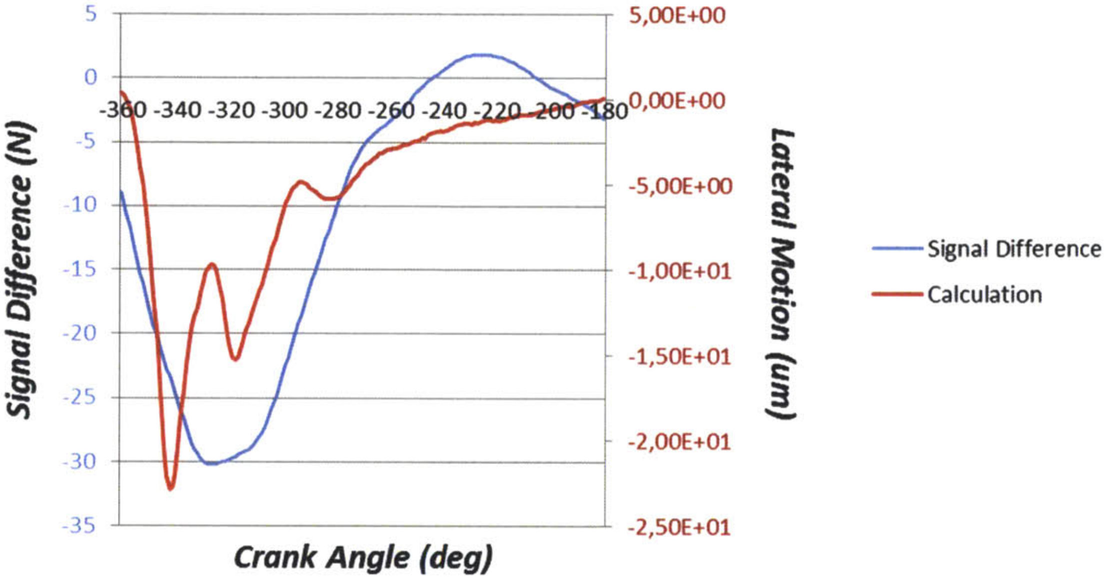

Figure 3.16 – Intake Stroke

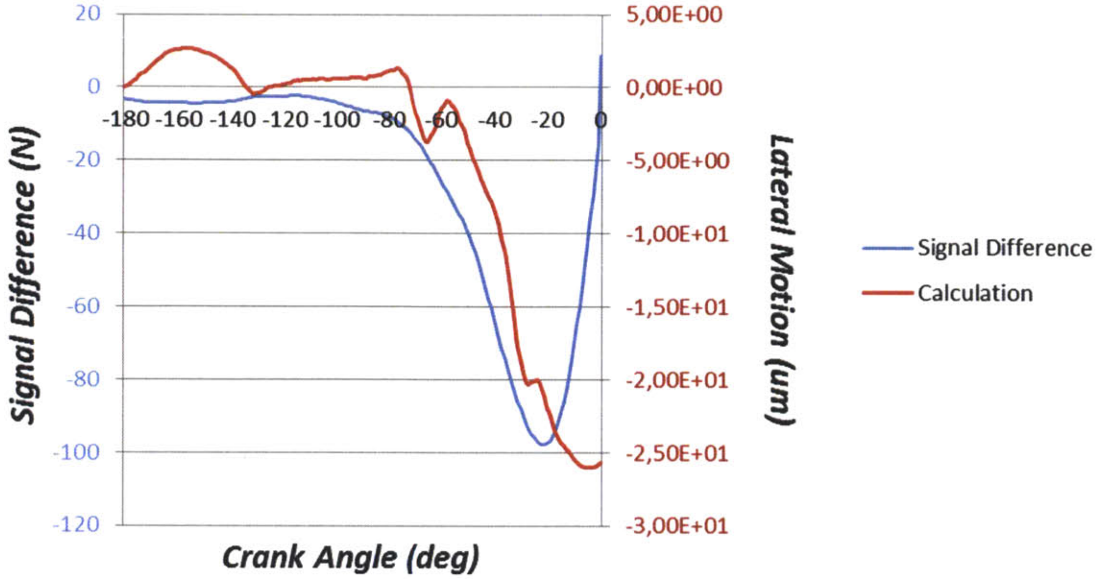

Figure 3.17– Compression Stroke

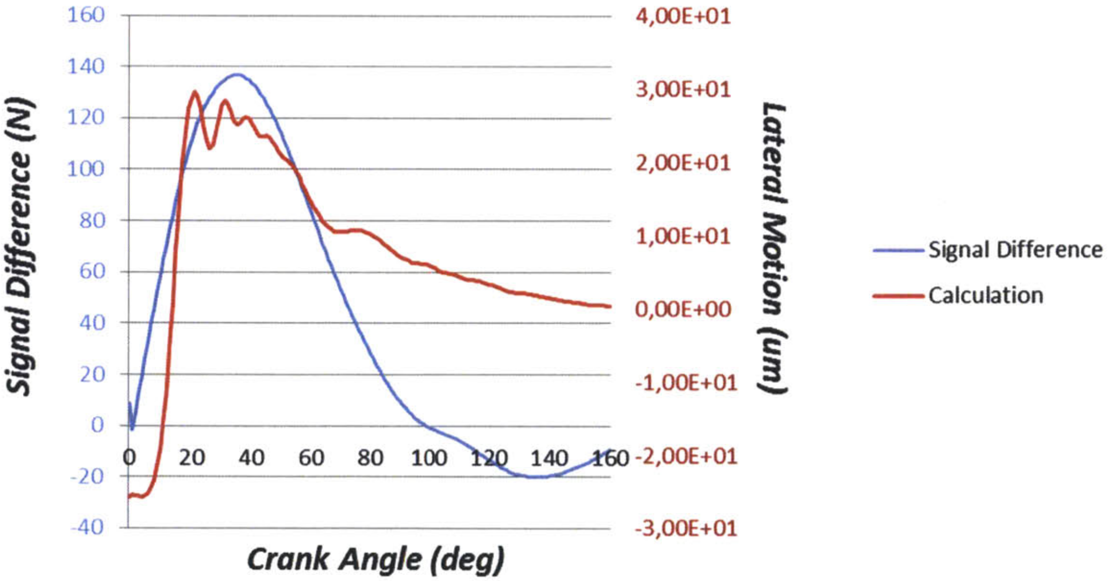

Figure 3.18 – Expansion Stroke

Looking at the figures the trend are well matched, especially during intake and compression stroke.

In conclusion, this study is, again, not pretended to be a way to validate the secondary motion calculation of the model, but it represents a way to check that the results are reasonable. Furthermore, such use of the sensors has been included in this thesis as it could be of inspiration for other different and interesting analysis.

Chapter 4

Piston's skirt pattern analysis

4.1 Skirt patterns

Among all the applications of the code, probably the most interesting has been the study of skirt patterns. With the advancement of manufacturing processes in producing pistons, coating patterns can be made quite easily. There has been a great interest to optimize the skirt design to reduce the friction without introducing negative effects on other behaviors associated to the piston secondary motion. Figure 4.1 shows an example of different coating patterns on the piston skirt.

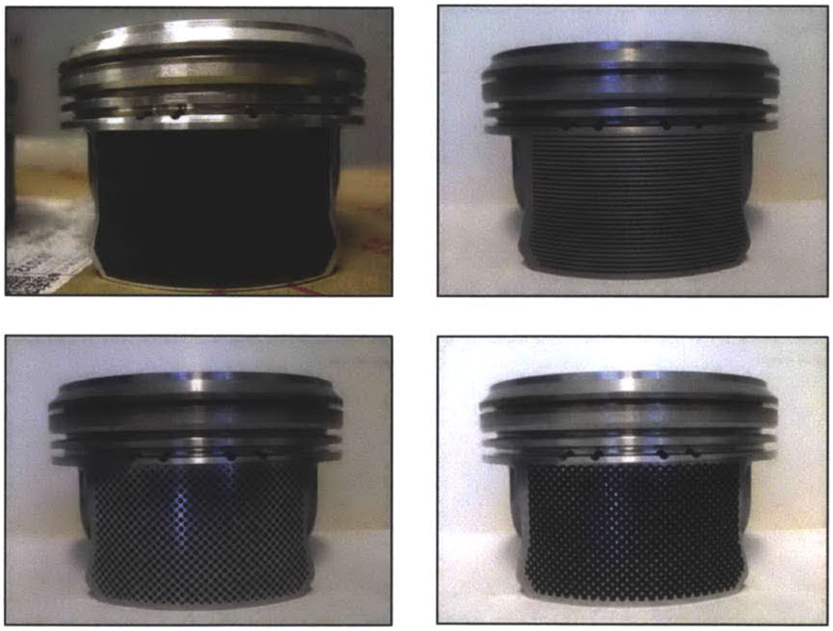

Figure 4.1 – Piston's skirt pattern prototyped

In order, top left picture shows a so called baseline piston; top right picture shows a "rows" pattern, as the name says the pattern is formed by parallel horizontal lines of coated material; bottom left picture shows a "dots" pattern, formed by a grid of coated dots; bottom right picture shows a "voids" pattern, which is essentially the inverse of the dots pattern. To be precise, the actual prototypes are only the last three. The baseline piston, in fact, has for long been used, because the coated material, softer than aluminum or steel, will accommodate the conformation of the skirt profile to the liner, simplifying the design of the piston's skirt, and it also has a lower boundary friction coefficient.

Parallel efforts have been made on the measurement side to examine the effects of different coating patterns on friction using a floating liner engine and on oil transport by visualizing the evolution of the oil accumulation with two dimensional laser induced fluorescence technique [6]. This work will focus on the simulation of these patterns with the model, in order to gain a better understanding of their performances. This chapter will first summarize the calculation results on the skirt designs shown in Figure 4.1. Then, new geometrical patterns are proposed to give better performance in friction without increasing the magnitude of the secondary motion.

4.2 Skirt FMEP results from the model

The main purpose of these calculations is to understand the correlation between frictional losses and the geometry of the pattern. From the beginning, the problem has been approached trying to highlight the hydrodynamic response of the patterns, which is believed to be the main cause of differences among them.

This strategy is applied by testing features of two different sizes (for dots, for example, the diameter tested was 2.5 and 1 mm); an example is shown in Figure 4.2. The purpose is to study the influence of the features' dimension on oil transport and lubrication. Secondly, two different thicknesses of coating material, namely 10 and 5 μm, are tested, using an oil supply to the system of $5\mu m$ each revolution. This is a fairly dry condition, but it is chosen to accentuate the differences between patterns' thicknesses.

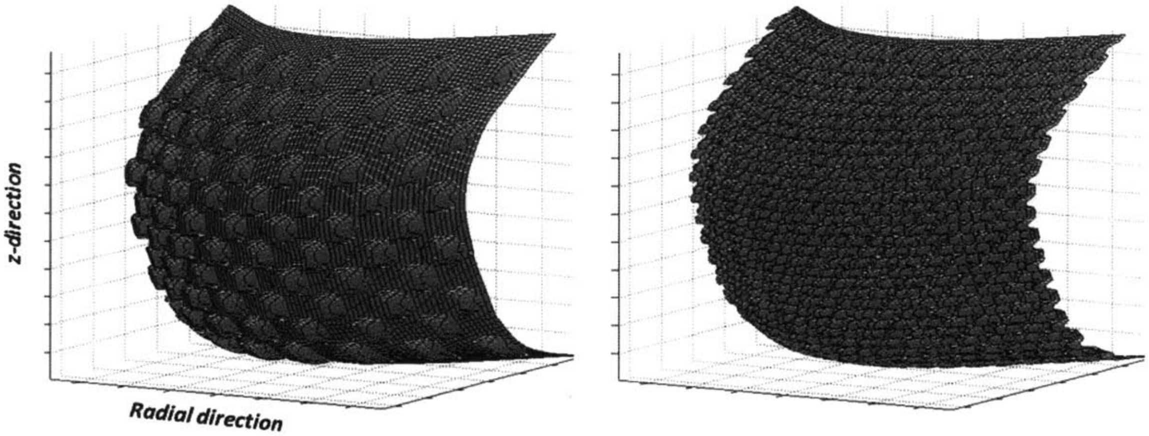

Figure 4.2 – Patterns with different features' size – Dots pattern

A note on the engine and running condition simulated for this study is necessary. Unfortunately, at the time these calculation were performed, a complete data set was only available for a racing engine. Nonetheless, the physics contributing to the effects of the patterns for the high speed operation is similar to low speed.

Another important concept to keep in mind, before showing the results, is that the nominal piston's diameter is the same for all designs, but if a pattern is applied to the piston's skirt, the clearance volume will be different with respect to the baseline piston. Specifically, since the coated material increases by several microns the radius of the skirt, the baseline piston would have the smallest clearance volume, whereas, the other designs would have region on the skirt, where the coated material has been removed, increasing the local clearance. Figure 4.3 shows, as an example, a comparison between baseline piston and dots pattern. This specific characteristic will change the space available to store oil over the skirt region and it drastically affects the hydrodynamic response of each design.

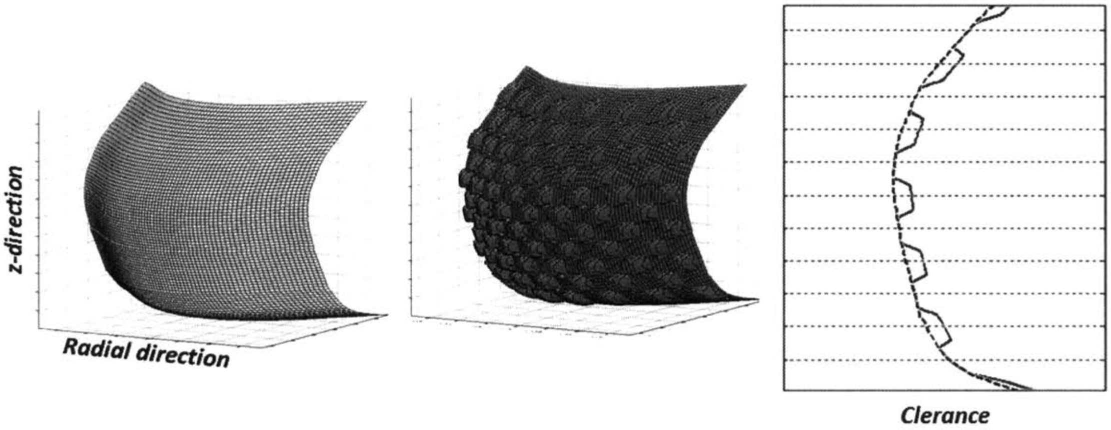

Figure 4.3 –Skirt's center cross section – Baseline and dots pattern

The running condition at which the simulations are executed is full load with a peak cylinder pressure of 95 bars at 16000 rpm. The first pattern analyzed will be the dots pattern, as the discussion brings up good points to understand the behavior of patterns in general. The first result shown is the skirt FMEP comparison with the baseline piston. Remember that the model does not include ring friction, therefore the FMEP calculated only accounts for skirt and lands frictional losses. Also, note that the actual values cannot be released for confidentiality reasons, nonetheless, the bars are proportional to actual values.

Looking at Figure 4.4, the baseline piston has a much smaller FMEP, compared to the other patterns. Also, we can note that the losses decrease if the coated material has smaller thickness and if the features are finer. This trends are directly correlated with the hydrodynamic response of the patterns.

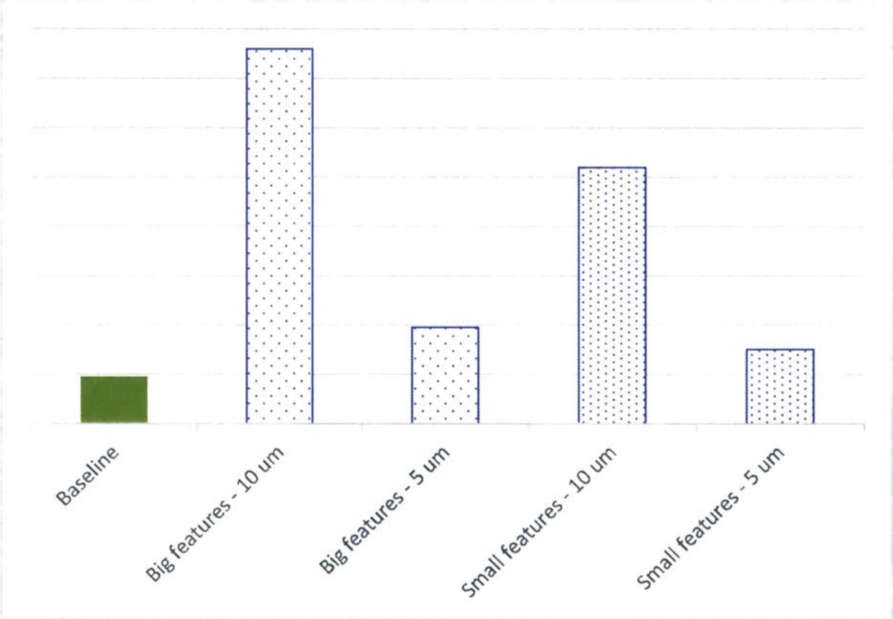

Figure 4.4 – Skirt FMEP comparison between baseline and dots pattern

Figure 4.5 shows the friction force comparison during a cycle, in the case of big features and $10\mu m$ thickness of coating material. It is apparent that the dots pattern causes a much higher friction than the baseline piston in some portion of the cycle. Large skirt friction forces for the dots pattern are a result of direct solid-to solid contact between the skirt and liner. Figure 4.6 shows the average contact pressure on the thrust side of the dots patterned skirt during the expansion stroke, which is the stroke with highest losses. The baseline piston does not experience contact at all, whereas the dots pattern presents important solid to solid contact.

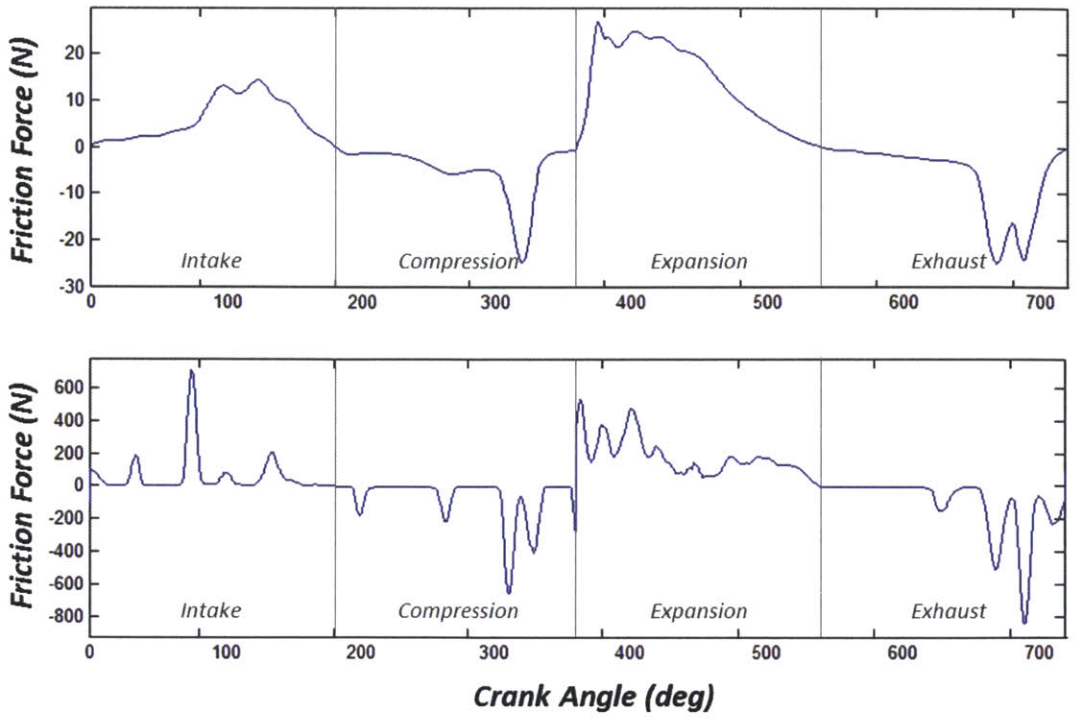

Figure 4.5 – Friction comparison
Baseline (top) – Dots, big features, 10um (bottom)

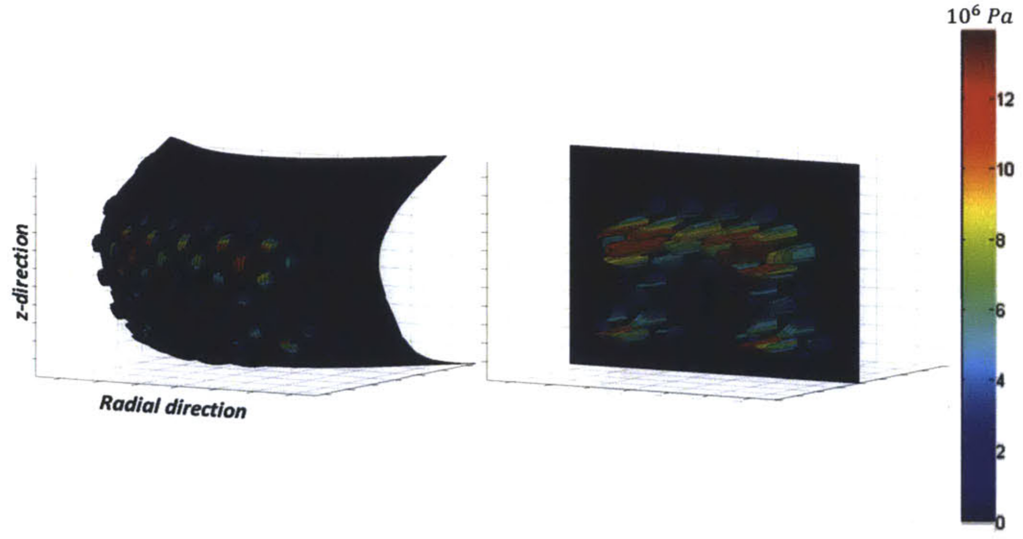
10^6 Pa
12
10
8
6
4
2
0
z-direction
Radial direction

Figure 4.6 – Dots pattern
Contact regions (left) and average contact pressure (right)
Expansion stroke - Thrust side

This difference is mainly caused by the hydrodynamic pressure generated on the skirt. The baseline piston, in fact, does not present solid to solid contact because the hydrodynamic pressure generated on the skirt is sufficient to balance the side force. Using the dots pattern, however, even if the side force does not change, the hydrodynamic pressure generate cannot alone balance the force, therefore the piston enters in contact with the liner. If we calculate the force generated by the hydrodynamic interaction between skirt and liner during the expansion stroke, the baseline piston generates an average force 96% greater than the one generates using dots pattern. This difference is correlated to the way the oil distributes over the skirt as illustrated in the following figures. Figure 4.7 and 4.8 shows, on the left, the regions on the skirt at thrust side that, on average, are fully flooded, meaning completely filled with oil, and where hydrodynamic pressure can be generated. Blue color indicates regions where the flooded condition is never achieved, red color indicates regions usually flooded during expansion stroke. On the right, the average hydrodynamic pressure distribution over the skirt, always at thrust side, is shown.

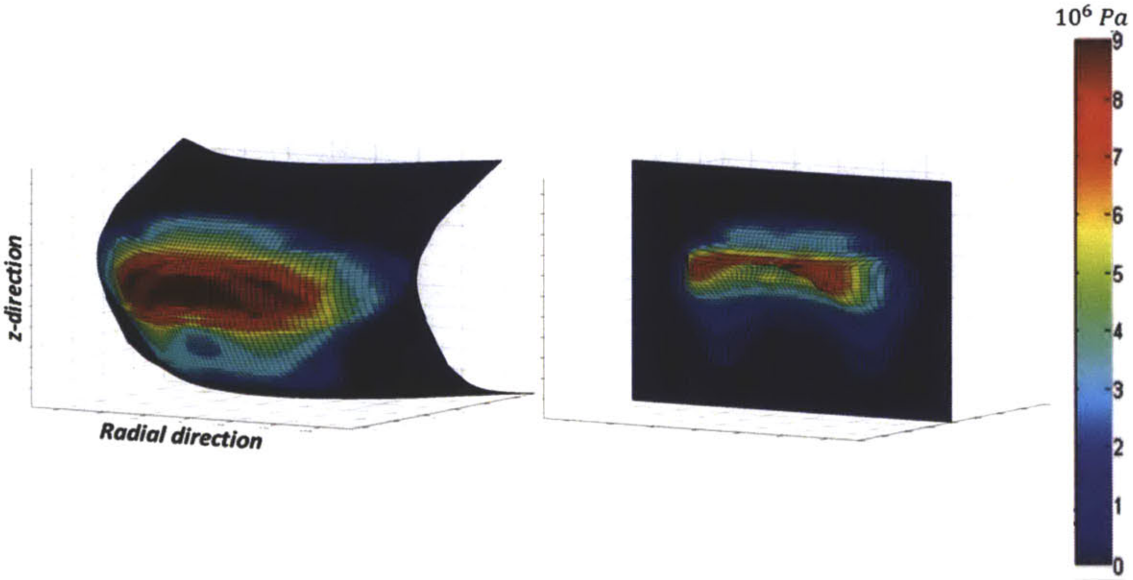

Figure 4.7 – Baseline piston
Average fully flooded regions (left) and hydrodynamic pressure (right)
Expansion stroke - Thrust side

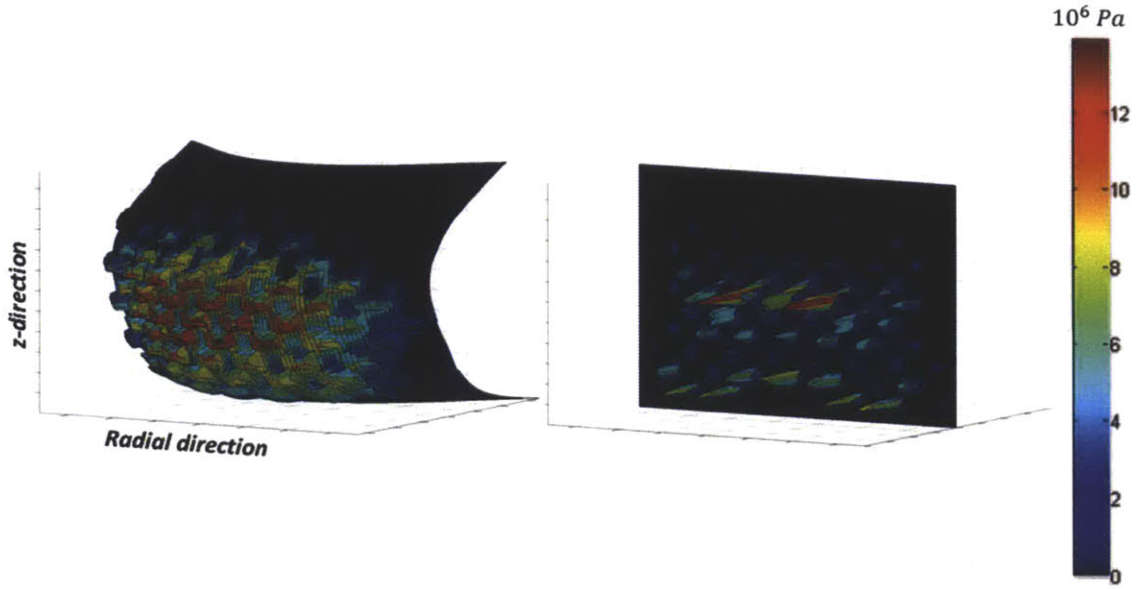

Figure 4.8 – Dots pattern
Average fully flooded regions (left) and hydrodynamic pressure (right)
Expansion stroke - Thrust side

Intuitively, the best way to generate hydrodynamic pressure is to concentrate the oil in a specific region on the skirt, because a continuous puddle is needed in order to create high pressures on an extensive region. This is, in fact, the case for the baseline piston. On the other hand, the presents of particular patterns, like dots, creates rather severe discontinuity of the skirt's profile, and it is much more difficult for the oil to concentrate in a specific region, because it either tends to accumulate below each dot or around them. This is counterproductive in terms of hydrodynamics, in fact, the pressure created is overall smaller in magnitude and non-uniformly distributed. Without specifically looking at the pattern's geometry, this behavior is related to the increase in clearance volume, since the oil tends to fill the space made available between the features rather than lubricate the components.

The weaker hydrodynamic pressure generation ability of the dots pattern, also greatly affects the secondary motion of the piston, which becomes much more unstable and oscillating. Figure 4.9 shows the lateral motion and the tilt angle comparison. For the first, positive values indicate motion towards thrust side, for the second, positive values indicate tilting of the top land toward anti-thrust side.

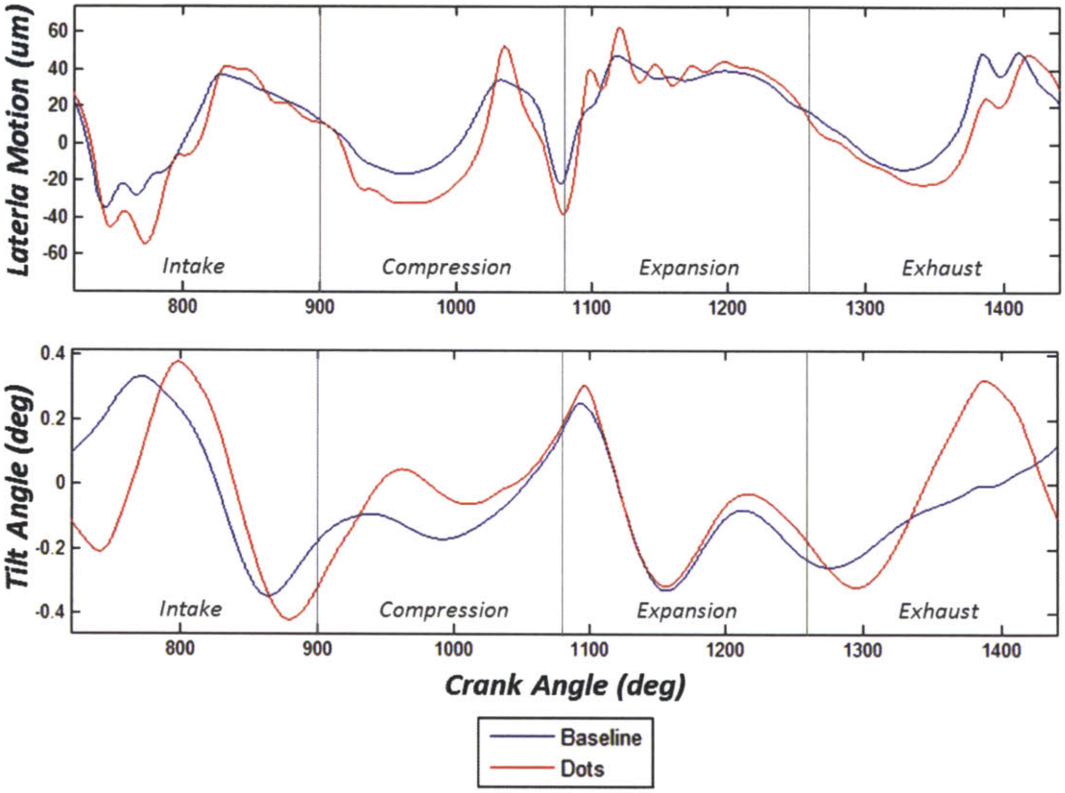

Figure 4.9 – Lateral motion and tilt angle comparison

In regards to the lateral motion, the dots pattern seems to follow the general trend of the baseline but with important oscillations. As for the tilt angle, it is completely unstable, it does not seem to follow a specific trend and its magnitude is much bigger if compared with the baseline's behavior.

This instability is connected to the way the side force on the piston is balanced. In general, generating hydrodynamic pressure on the skirt through lubrication creates a reaction force that can rapidly counter balance the side force, if the skirt is properly lubricated. If, however, the hydrodynamic pressure generated is weak, the skirt will balance the side force with solid to solid contact. In this scenario, since the piston will need to move further toward the liner in order to find contact, the response to the side force is delayed and the magnitude of lateral motion is increased. Since the friction force due to contact is much stronger than that due to shear stresses, the tilting motion of the piston is emphasized amplitude as well. As a result, the piston becomes more unstable. Further evidence can be seen from Figure 4.10 that the inertia force of the piston from its lateral acceleration has higher magnitude and more pronounced oscillatory behavior in the case of the dots patterns.

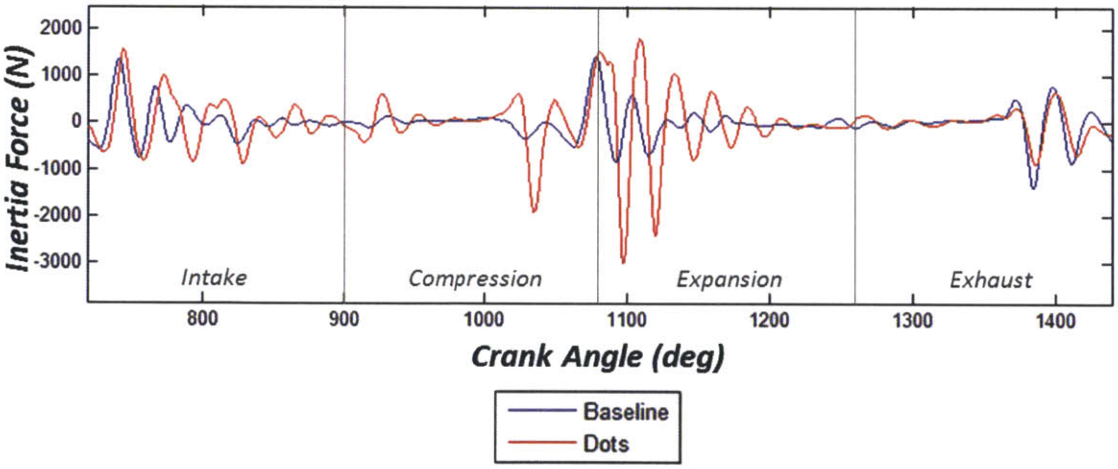

Figure 4.10 – Inertia force comparison

Both frictional losses and secondary motion gets closer to the behavior of the baseline piston, if finer features of smaller thickness are used. This is again correlated to the hydrodynamic response of the pattern and to the clearance volume and space available to the oil, which in these cases would decrease, improving the capacity to create a uniform oil film on the skirt and balance the side force with hydrodynamic pressure.

The analysis made for this first pattern is valuable also for the study of other patterns. The skirt FMEP results for the voids and rows pattern, compared to the baseline piston, are reported in Figure 4.11.

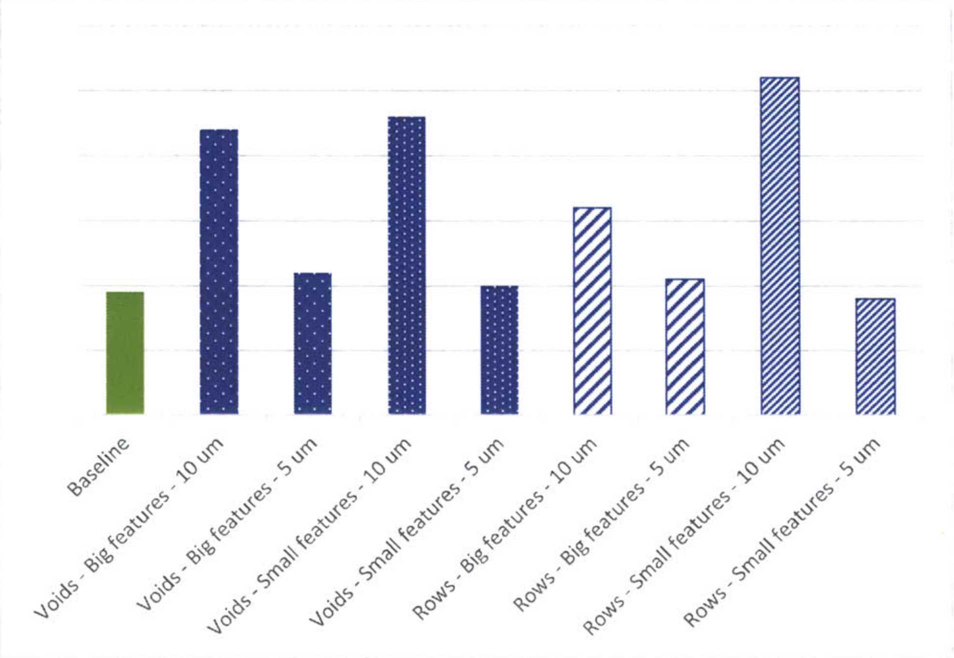

Figure 4.11 – Skirt FMEP comparison between baseline, voids and rows patterns

Also in this case the frictional losses are in general greater than the baseline piston, but they are definitively smaller if compared to the dots pattern. The FMEP always reduces using finer features and smaller thickness of the coating material, and in particular for the rows pattern the losses are slightly smaller than the baseline piston. The causes that lead to higher friction are always connected to the hydrodynamic response of the patterns and to the way the side force is balanced as discussed earlier in the section, therefore the cases of worse performance will be not analyzed for brevity. Nevertheless, it is interesting to briefly focus, as last topic of this section, on the cases that present a similar or better performance than the baseline piston and understand what the difference with respect to the dots pattern is.

The patterns studied for this discussion are the voids and rows pattern, with finer features and coating material thickness of $5\mu m$. In order to understand why these cases have close performances to the baseline piston, we need to look at the way the oil distributes over the skirt. To do so, again, the regions that on average are fully flooded during the expansion stroke at thrust side are presented in Figure 4.12.

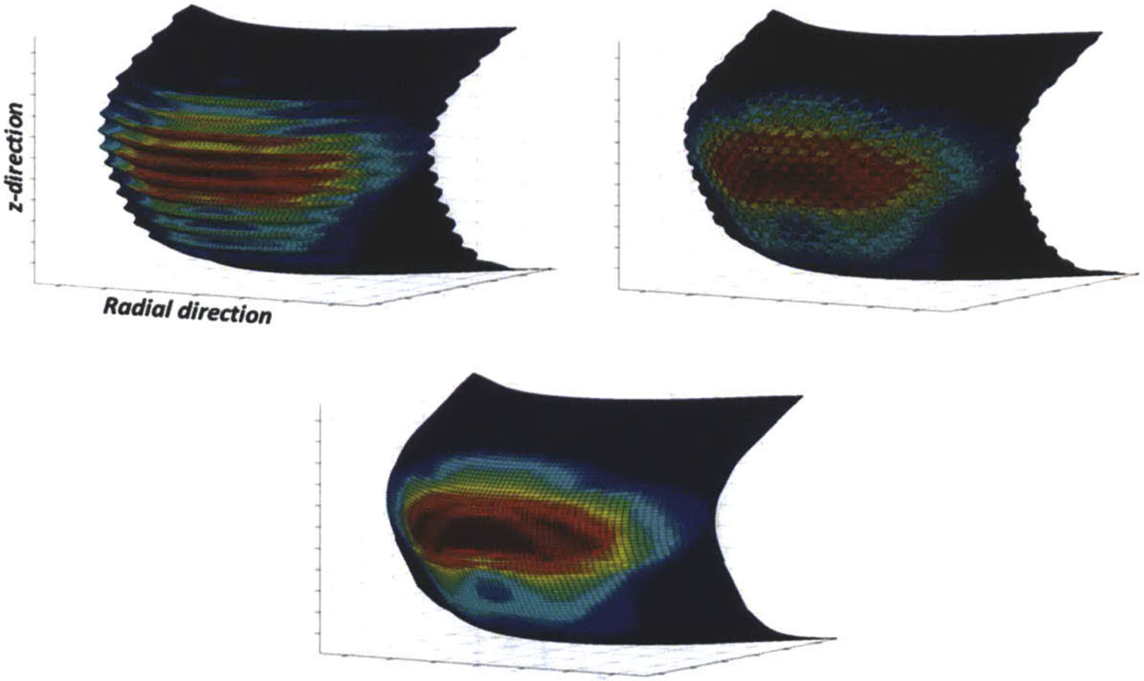

Figure 4.12 – Average fully flooded regions
Rows (top left), voids (top right) and baseline piston (bottom)

From the figures we can see that the flooded regions are similar to each other, even if the presence of the features is visible. This makes the hydrodynamic behavior also similar, in fact, the solid to solid contact for voids and rows pattern is very small, meaning that the hydrodynamic pressure generated can itself balance the side force. This comparison explains the similar performances. As we have previously described however, this is not the case for the dots pattern, and the cause is related to the way the oil tends to redistribute over the skirt.

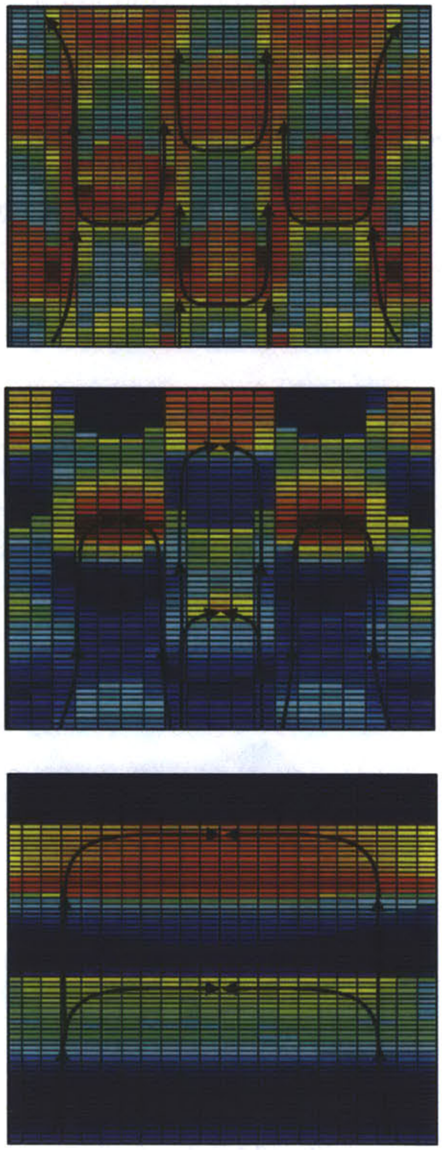

Figure 4.13 – Oil paths for dots, voids and rows pattern

Examining the average fully flooded region during the expansion stroke, it is possible to highlight the paths that the oil tends to follow. Figure 4.13 shows these path for every pattern. As already explained previously, the increase in clearance volume generally makes more space available on the skirt for the oil, however, the specific geometry of the feature will influence the way oil moves over the skirt and this can make an important difference. Qualitatively, we can see that for the dots pattern, the oil tends to slightly accumulate below the dots, but most of it is able to find a path to reach the top of the skirt because the geometry of the features is not able to block its motion. The consequence is that the oil will mostly accumulate in the chamfer region and will not be available to lubricate the skirt. The situation is different for the other patterns, in which the feature's geometry is promoting the accumulation of oil, for example inside the voids or between rows, so that it can be available to lubricate the skirt. Note that this tendency to accumulate oil is productive only if the increase in clearance volume, in relation to the oil supply, is not excessive.

In summary, none of the patterns has given a better performance than the baseline for the engine and operating condition studied. On the other hand, this study has provided the opportunity to understand what can be productive and counter-productive by including patterns on the piston's skirt. The next section will focus on exploring new types of patterns and their potential for skirt friction reduction.

4.3 New pattern design – Racing engine

The use of patterns has been proposed, since the beginning, to reduce frictional losses, but this has not been achieved yet with the designs tested. The concept of creating particular geometries on the piston's skirt can however be promising, and the use of the model would be extremely helpful to that end, since any design can be first simulated, in order to study its behavior, and then prototyped and tested experimentally, saving time and money. This section will focus on the development of a new pattern and the results from the model will be illustrated.

In order to understand how the new pattern has been conceived, it is necessary to emphasize a few basic concepts to keep in mind. As we have discussed in the previous section, the presence of a pattern can drastically worsen the hydrodynamic behavior of the skirt. In particular this is related to the increase in clearance volume, to the way the oil tends to distributes over the skirt and to the discontinuity that a pattern gives to the skirt profile, which affects the hydrodynamic lubrication. If these negative effect can be limited, the pattern can actually be used to decrease frictional losses by promoting the accumulation of oil on the skirt and enhance its lubrication.

The new pattern, in particular, has been designed taking into account a couple of problems that could be resolved with the use of particular geometry on the skirt. The first issue discussed analyses the oil that enters or exits the lower boundary of the skirt. In general the oil accumulated on the liner is a good form of oil supply for the piston, since it enters and accumulates in the skirt region during a down-stroke, creating a favorable condition for lubrication. The situation is however different during an up-stroke, in which the oil, accumulated in the previous down-stroke, will be rapidly released on the liner's surface, as the piston proceeds in its motion, reducing the amount of lubricant available to the skirt. Figure 4.14 schematically shows this concept. The second issue is related to the skirt profile. Generally, the skirt profile, as shown in Figure 4.15, has a point of minimum clearance around the center of it, in which the highest hydrodynamic pressure and shear stresses are generated. The new pattern has been designed in order to try to address these issues.

The idea is to create a feature that promotes oil accumulation on the skirt, towards the point of minimum clearance, and helps to retain oil during an up-stroke. This needs to be done without creating excessive discontinuity of the skirt profile and limiting the effect of increase in clearance volume. The very first pattern designed to accomplish to this objectives is schematically illustrated in Figure 4.16.

The pattern is really simple and it is ideally composed of a single curved line of coated material on thrust and anti-thrust side. The purpose of the different configurations is that at thrust side, where the losses are usually important during the expansion stroke, the pattern will help to accumulate oil near the point of minimum clearance, whereas at anti-thrust side, which usually is the side that experiences important losses during up-strokes, the pattern will retain oil on the skirt.

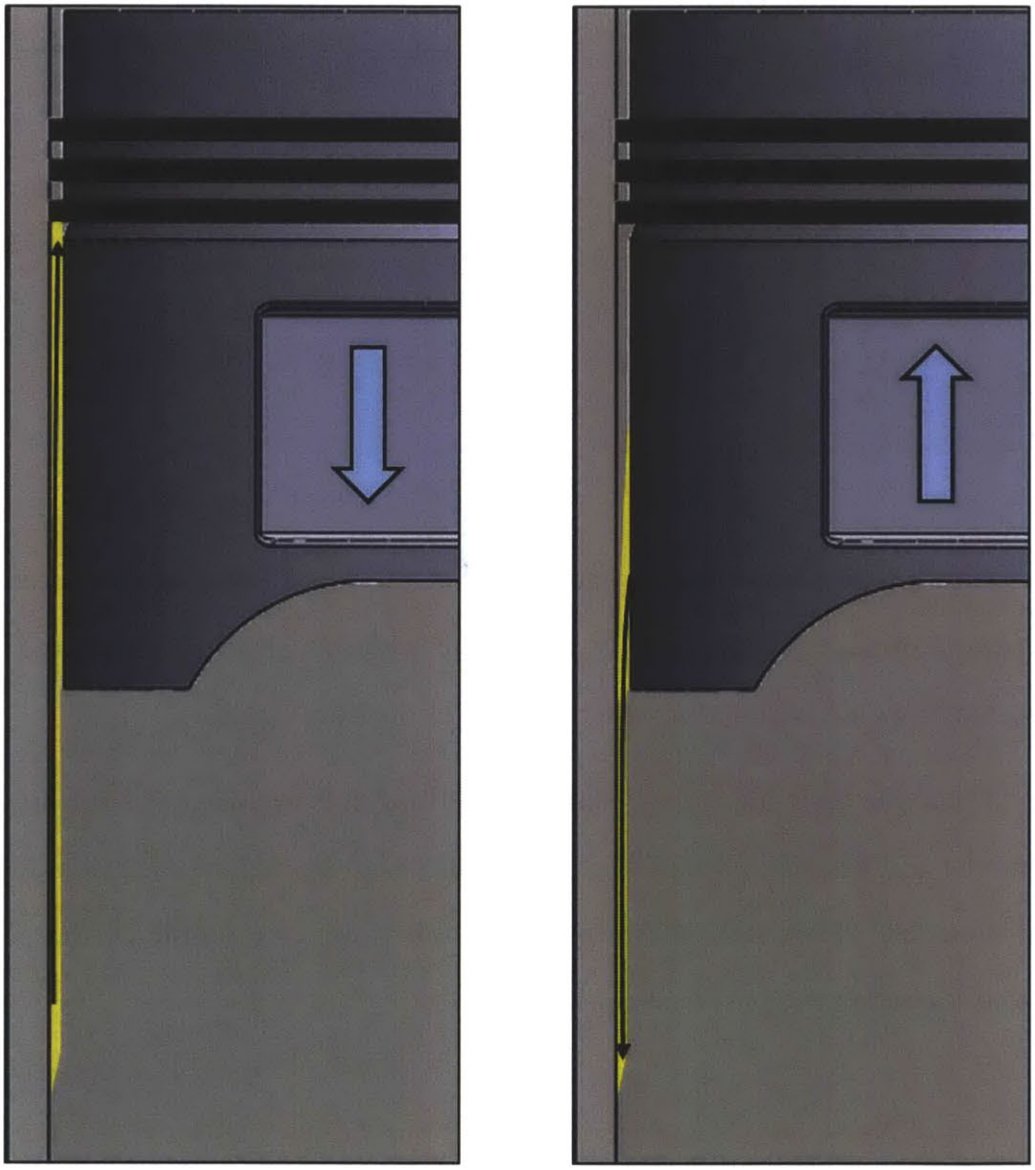

Figure 4.14 – Oil supply to skirt from liner, down-stroke and up-stroke

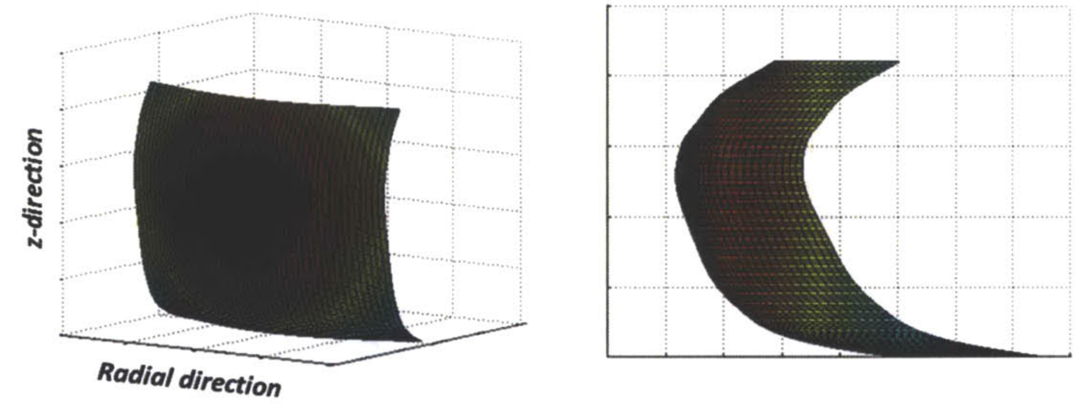

Figure 4.15 – Usual skirt profile

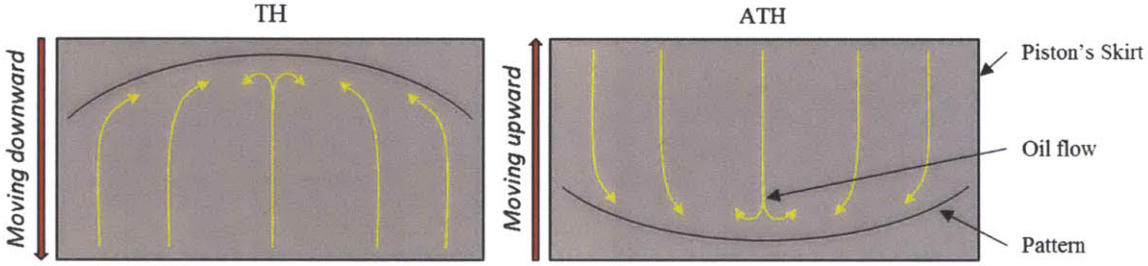
TH
ATH
Moving downward
Moving upward
Piston's Skirt
Oil flow
Pattern

Figure 4.16 – New pattern's schematic

One particularity of this pattern is that the features are not repeated. The repetition, in fact, can negatively affect the purpose of the pattern and more importantly would create more discontinuity of the skirt's profile.

Once the basic idea of the pattern is defined, it is necessary to introduce it in the model and describe its actual profile. Figure 4.17 shows how the initial idea has been modeled. Please note that the figures only shows the profile of the pattern, without including the profile of the skirt.

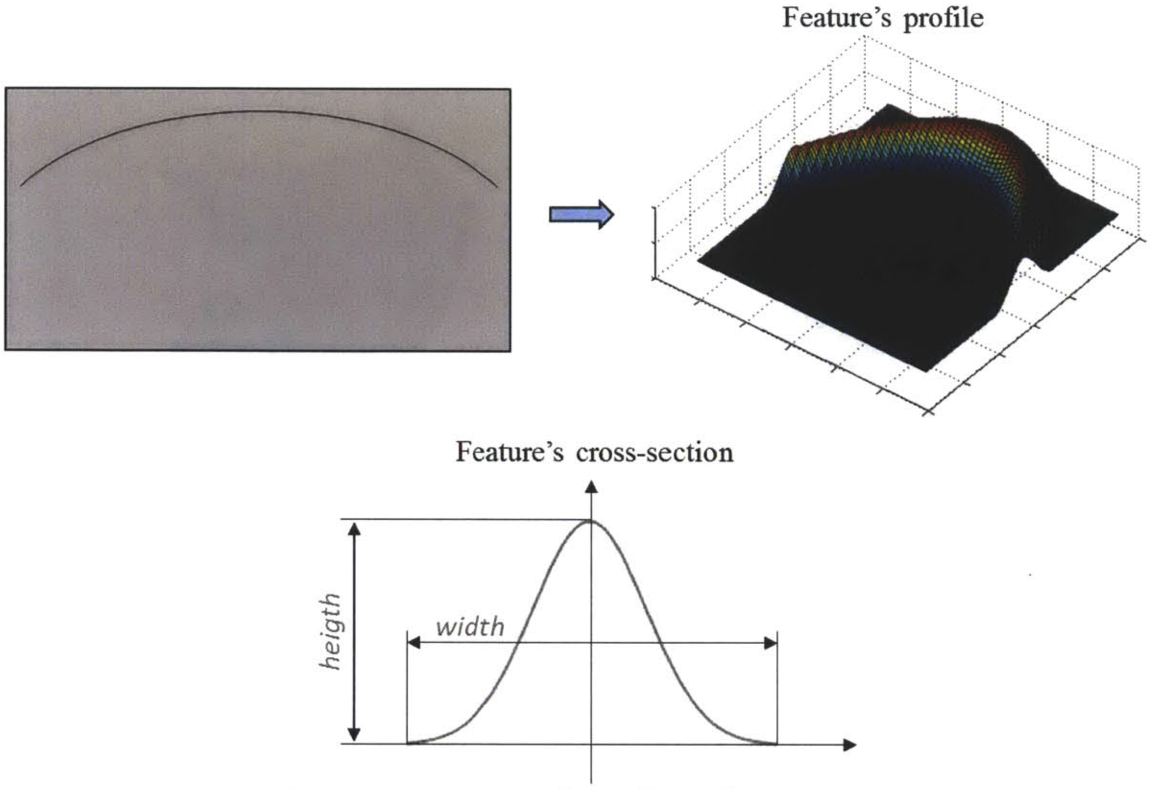

Figure 4.17 – Feature's profile and cross-section

In this case the cross section of the feature has been smoothened to improve its hydrodynamic behavior. Also, the cross section is defined by height and width; the height represents the thickness of the coated material and is kept fixed in the calculation, however, the width has a great influence on the results, in fact, its influence will be studied to find an optimum value. An example of the skirt profile with the inclusion of the pattern is shown in Figure 4.18.

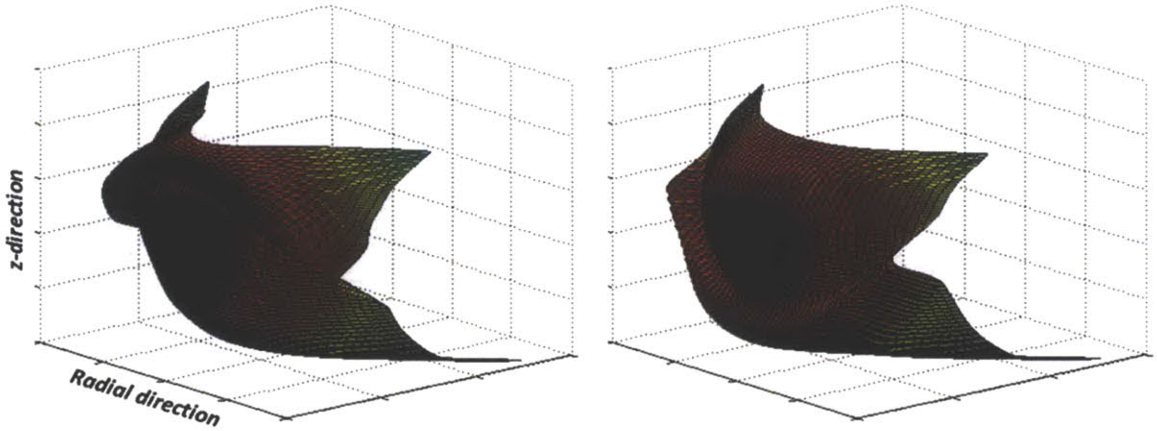

Figure 4.18 – Example of thrust side and anti-thrust side with the new pattern

The calculations are again executed simulating a racing engine, at 16000 rpm, full load. The first result presented is the friction force comparison between baseline and the new pattern.

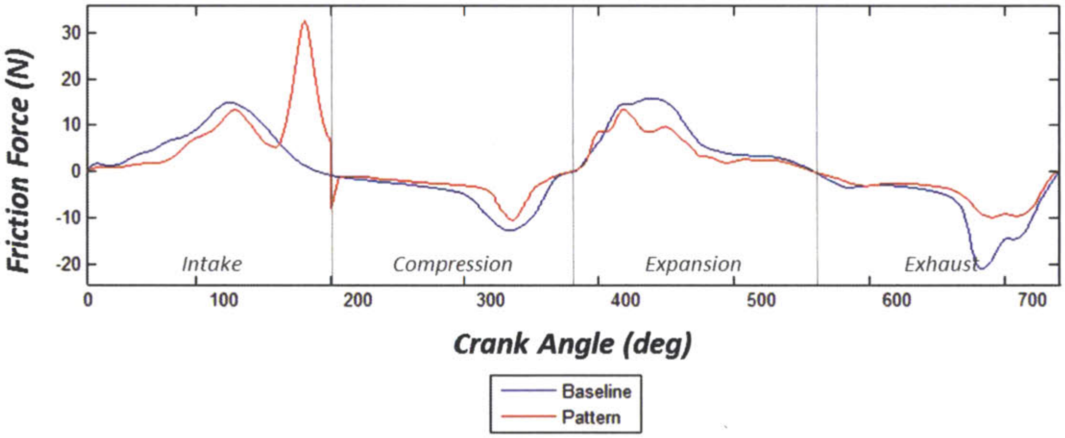

Figure 4.19 – Friction force comparison

Interestingly, the friction force has resulted reduced with the use of the pattern, specifically with a skirt FMEP decreased of roughly 29%. Furthermore, looking at the hydrodynamic pressure distribution and fully flooded regions on the skirt, represented in red, in Figure 4.20 and 4.21, we can see that the features are accomplishing to their purpose. During the expansion stroke, at thrust side, the feature is succeeding to accumulate oil towards the center of the skirt, which is where the clearance is usually smaller, whereas, during the compression stroke, at anti-thrust side, the feature is helping to retain oil in the skirt region. Also, calculating the contact friction, it has been reduced by 13%.

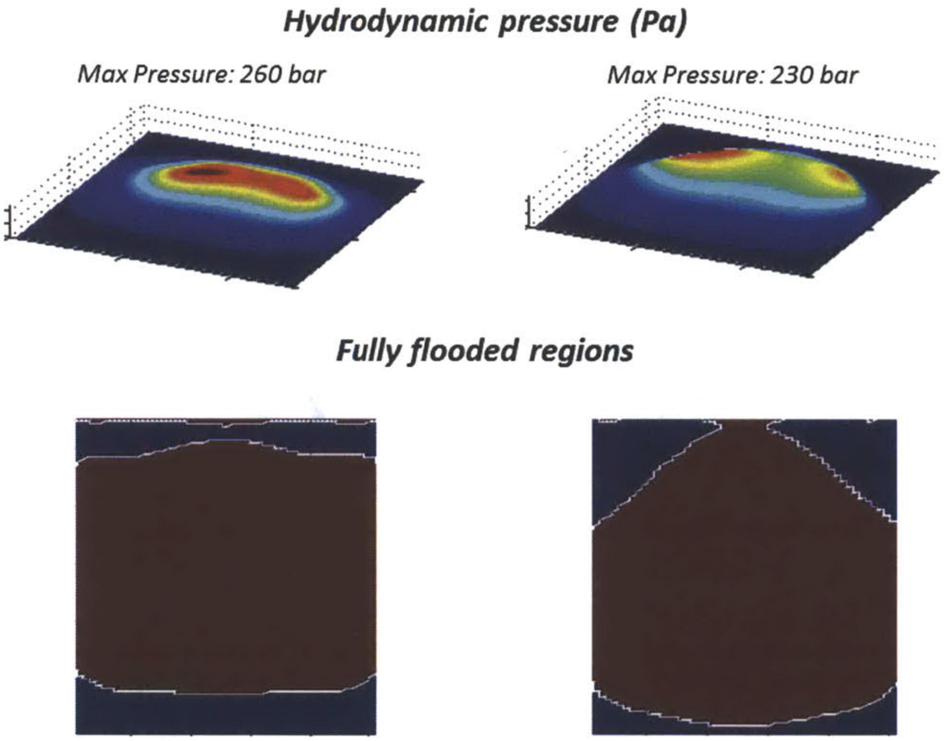

Figure 4.20 – Hydrodynamic pressure and fully flooded regions
Thrust side - Expansions stroke - Baseline (left) new pattern (right)

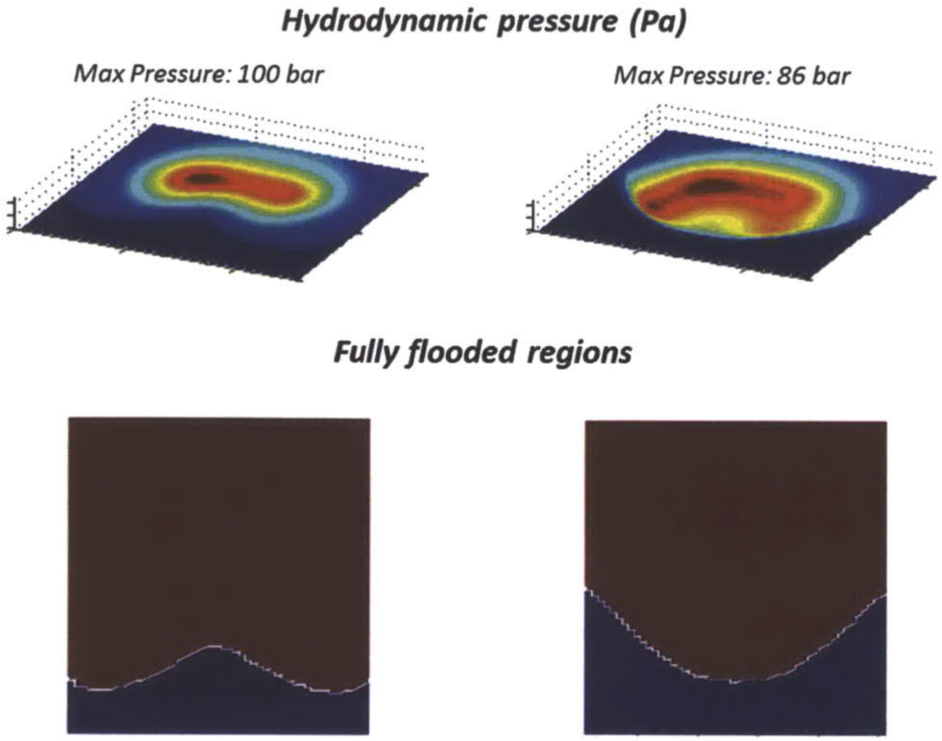

Figure 4.21 – Hydrodynamic pressure and fully flooded regions
Anti-thrust side - Compression Stroke - Baseline (left) new pattern (right)

A further improvement can be done by studying the influence of the feature cross-action's width. This characteristic of the feature, in fact, affects the solid to solid contact that the skirt can experience. Figure 4.22 shows the friction force for the optimized pattern, and we can see in Figure 4.23 that the contact experienced at the end of the intake stroke in the previous case is much less pronounced here. Calculating the skirt FMEP for this case, it is further decreased by 35%.

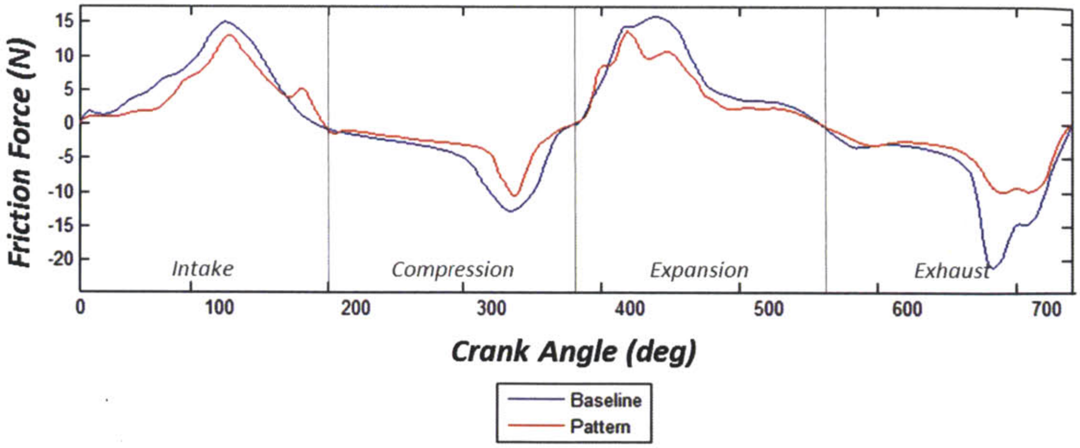

Figure 4.22 – Friction force comparison for the optimized pattern

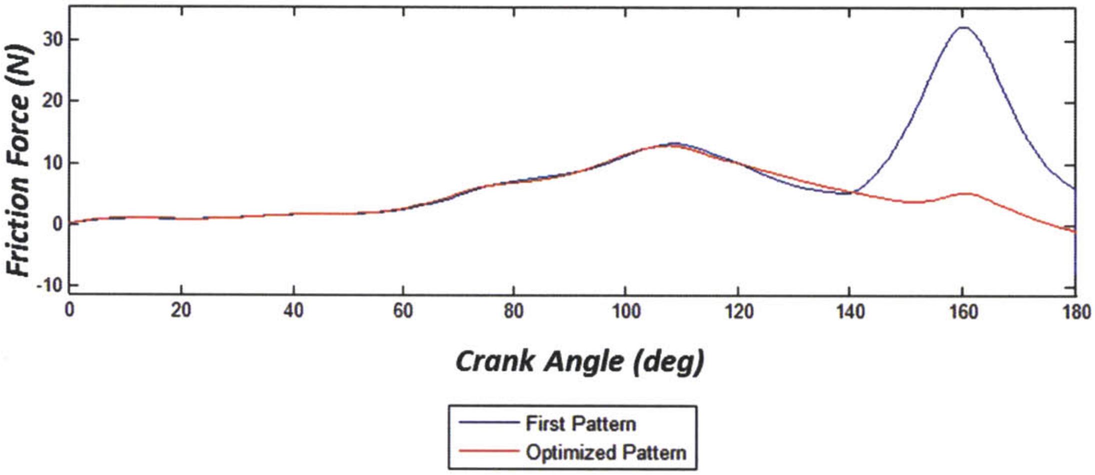

Figure 4.23 – Pattern's friction force comparison – Intake stroke

In conclusion, this study has proven that it is possible to design a skirt's pattern that can help to reduce frictional losses. The study, however, is not completed, in fact, more alternatives can be tested and different engines need to be simulated.

4.4 New pattern design – Passenger car engine

The interesting results achieved studying the performances of the new pattern on a racing engine, have brought attention to the concept of this design, and its application to passenger can engines needed to be covered. Luckily, soon after the conclusion of this investigation, the data for the 2D LIF engine have come available and have been used for the calculations in this section. The running condition simulated is 2000 rpm, partial load.

The first result presented will illustrate the friction results calculated by applying the same pattern described in the previous section. Also in this case the skirt FMEP has been decreased, specifically by 36%. Figure 4.24 shows the friction comparison.

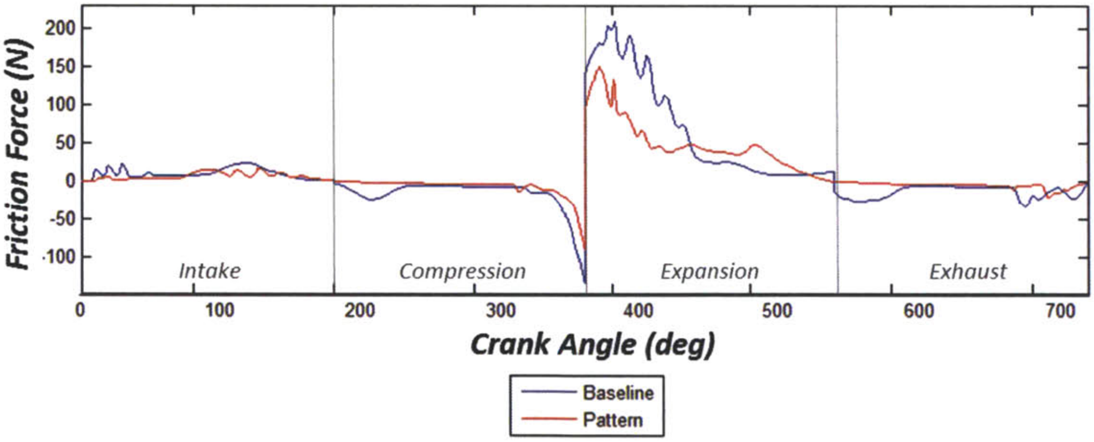

Figure 4.24 – Friction force comparison

This results can be further improved by studying the width of the pattern. However, other alternative designs can be tested, before analyzing the geometry of the pattern. For this purpose, the basic idea of the current pattern has been used to create other options that are a modification of the current design. Figure 4.25 shows the features' profile at thrust and anti-thrust of the two other patterns tested.

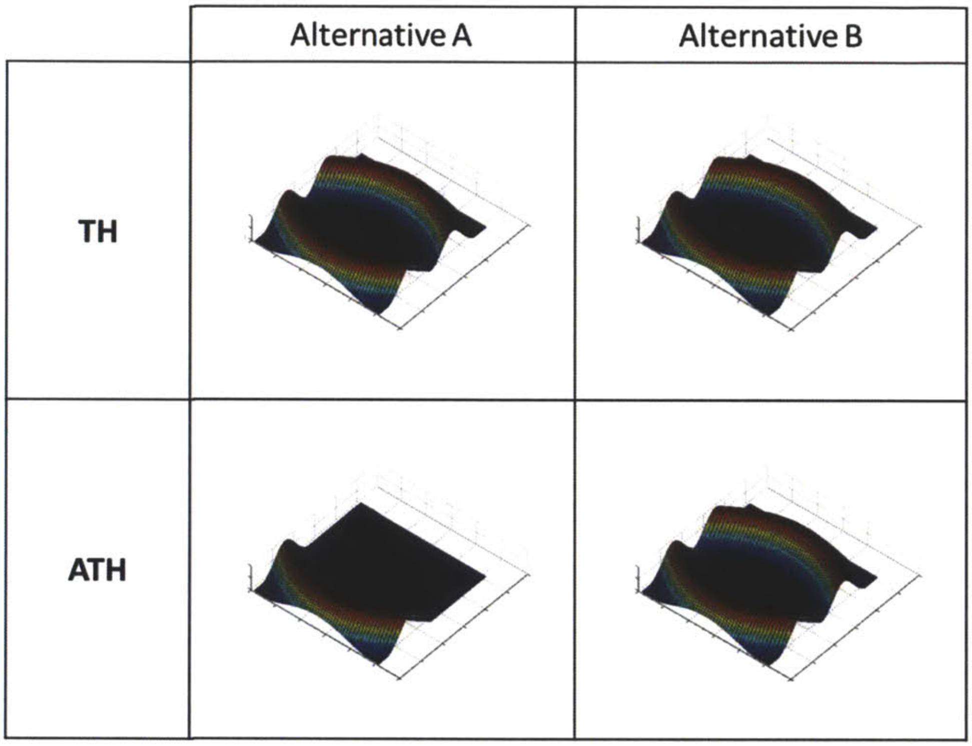

Figure 4.25 – New pattern's alternatives

Executing the calculation, the performances are further improved. Specifically, Alternative B have resulted to decrease piston's frictional losses by 41%. Optimizing then the width of the features, the skirt FMEP results reduced by 48%.

One concern related to the presence of the patterns is that the increase of clearance volume might affect the secondary motion of the piston, which can negatively influence oil consumption, especially if the tilt angle reaches significant magnitudes. Comparing the results for secondary motion, however, the differences between the baseline piston and the optimized pattern are negligible.

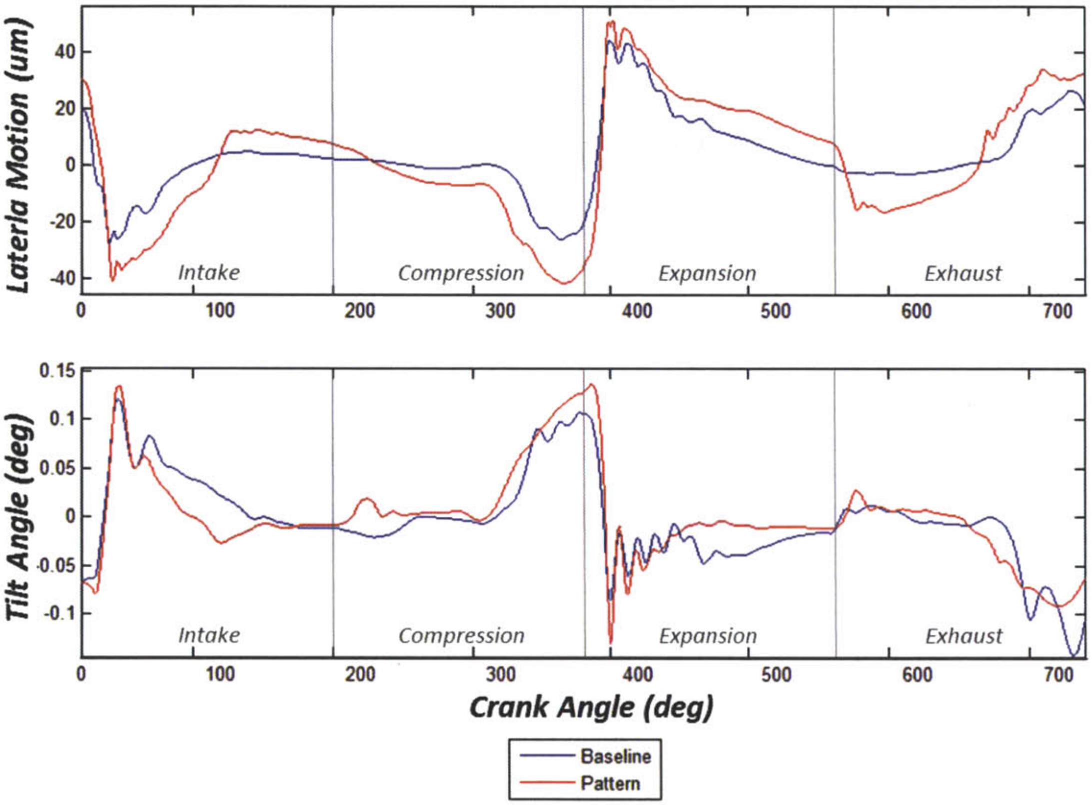

Figure 4.26 – Piston's secondary motion comparison

Secondly, since one of the purpose of the patterns is to hold or accumulate oil on the skirt, the amount of lubricant reaching the chamfer region of the piston might increase and this again represents a problem for oil consumption. Analyzing the average oil film thickness in the chamfer region, in fact, there are some point during the cycle in which the baseline present less oil in the chamfer region, especially at thrust side at the end of the intake stroke. This might be something to take into consideration when testing these patterns.

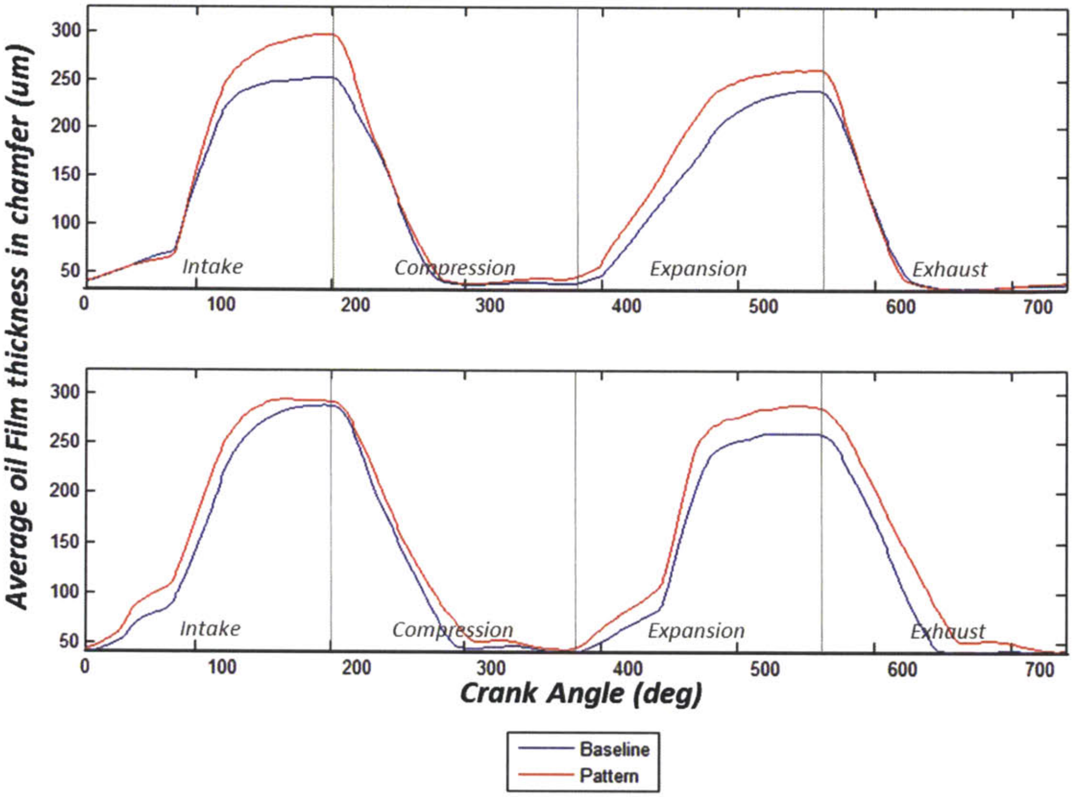

Figure 4.27 – Average oil film thickness in the chamfer region comparison Thrust side (top) anti-thrust side (bottom)

In summary, this chapter have proven that it is possible to design skirt's pattern that can help to reduce frictional losses and in particular the one described in this thesis has resulted to give really good improvement of the skirt FMEP. Certainly, Further simulation need to be done to access its behavior at other running conditions with different oil supply and this will be part of the future work. Nonetheless, even with the current results, our sponsors have expressed the interest to prototype the pattern and experimentally test its performances, in order to bring this design concept a step further.

Chapter 5

Conclusion

5.1 Development and application of the model

The first part of this thesis work has focused on improving the existing model, including some important phenomena that make the general physical description of the system better.

In the existing version of the model [4], the liner dynamic deformation was not included, however it can greatly affect the results. In particular, when the liner is rather flexible, its dynamic deformation can reach magnitude of $50-40\,\mu m$, influencing the secondary motion. Also, assuming the liner as a rigid component facilitate solid to solid contact, affecting the friction calculated.

A second major change is the calculation of viscosity considering temperature and shear-thinning effect. As it has been illustrated in Chapter 3, the viscosity can appreciably change during the cycle, due to different temperatures at TDC and BDC, and different shear rates over the skirt. Considering an average value of viscosity, which takes into account a low shear-stress and high shear-stress viscosity, does not allow to capture the real situation, in fact for example, solid to solid to contact at TDC and BDC is usually less if the viscosity is directly calculated, since in these points of the cycle the shear stress is almost absent and the real value of viscosity will be higher than the average value. On the other hand at mid-stroke, the actual value of viscosity can be less than the average value, resulting in less hydrodynamics friction. The downs side is that adding shear-rate and temperature influence on viscosity increases the computation time.

The second part of this thesis work mainly focuses on the application of the model, by studying the effects of geometrical features on piston secondary motion, skirt lubrication, and friction.

The comparison of calculation's results and experimental measurements, from the floating liner engine, have shown the importance to include temperature and shear-thinning effect on viscosity in the calculation, and have brought attention to the contact friction calculated in the simulations. At this stage, however, it is early to judge the accuracy of the code, since more cases need to be studied.

The skirt's pattern study has shown how the model can be used to help the design of piston's skirt. The discussion has demonstrated how the lubrication of the skirt can be greatly affected by the additional features to the existing profile. If the features introduce channels to ease the oil flows between the skirt and liner, filling the space made available, the hydrodynamic lubrication will be negatively affected and more solid-solid contact can occur. However, if the features promote oil accumulation on the skirt and do not create excessive discontinuities of the skirt's profile, the performances can improve. The new design presented, is an example of a good application of the pattern and represents a starting point in the process of better designing the skirt's profile.

5.2 Future work

The work done so far has definitively improved the way the model can realistically describe the power cylinder system, however, this process is not finished yet. As discussed in Chapter 2, the way the oil supply to the system is modeled is simplistic, in fact, how additional oil flows to the liner and how it is distributed obviously depends on the crankcase design and the behavior of the oil cooling jet, and this needs more work. Another topic of interest is the pin-piston lubrication.

Currently it is assumed that the interaction between pin and piston is frictionless, but it is not in reality. This particular phenomenon can affect the secondary motion of the piston, especially when the piston's primary acceleration is important, due to the friction at the pin bosses. This is a complicated system to describe, as it involves modeling the hydrodynamic lubrication and the oil supply of the pin, nonetheless, it is an important component to be studied in the future and included in the model.

With regard to the validation of the model, the study described in Chapter 3 is not completed. More running conditions need to be analyzed, possibly focusing on different pistons and keeping the ring pack unchanged, in order to highlight the friction differences that the piston only causes. Also the model itself needs to be provided of the missing data for liner's thermal and dynamic deformation, which may importantly affect the results.

Also the application of the model as a tool for piston's design needs to go forward. The studies presented in this thesis are specific to the skirt's patterns, however, a general and broad study to optimize the skirt's profile has not been done yet. So far the piston's skirt profile used has always been roughly the same, but a broad variety of options can be tested. This project needs to continue on studying the influence that every parameter that defines the skirt, such as profile, clearance volume, chamfer volume, skirt length or width, has on performances. The ultimate goal is trying to understand how frictional losses scale with the geometry of the piston.

References

[1] Heywood, John B., "Internal Combustion Engine Fundamentals", Mc Graw Hill, 1988.

[2] United States Environmental Protection Agency, "EPA and NHTSA Finalize Historic National Program to Reduce Greenhouse Gases and Improve Fuel Economy for Cars and Trucks", 2010.

[3] United States Environmental Protection Agency, "EPA and NHTSA Set Standards to Reduce Greenhouse Gases and Improve Fuel Economy for Model Years 2017-2025 Cars and Light Trucks", 2012.

[4] Bai, D., "Modeling Piston Skirt Lubrication in Internal Combustion Engines", PhD thesis, Massachusetts Institute of Technology, 2012.

[5] McClure, F., "Numerical Modeling of Piston Secondary Motion and Skirt Lubrication in Internal Combustion Engines", PhD thesis, Massachusetts Institute of Technology, 2007.

[6] Zanghi, E., "Analysis of Oil Flow Mechanisms in Internal Combustion Engines via High Speed Laser Induced Fluorescence (LIF) Spectroscopy", S.M. thesis, Massachusetts Institute of Technology, 2014.

[7] Senzer, E., "Oil Transport Inside the Oil Control Ring Groove and it's Interaction with Surrounding Areas in Internal Combustion Engines", PhD thesis, Massachusetts Institute of Technology, 2012.

[8] Przesmitzki, S.: “Characterization of Oil Transport in the Power Cylinder of Internal Combustion Engines during Steady State and Transient Operation”, PhD thesis, Massachusetts Institute of Technology, 2008.

[9] Li, Y., “Multiphase Oil Transport at Complex Micro Geometry”, PhD thesis, Massachusetts Institute of Technology, 2011.

[10] Kundu, Cohen, Dowling, “Fluid Mechanics”, Academic Press, 2012.

[11] Taylor, R. I., “Tribology and energy efficiency: from molecules to lubricated contacts to complete machines”, Faraday Discussions, 2012.

[12] Lee, D. T., Schachter, B. J., “Two Algorithms for Constructing a Delaunay Triangulation”, International Journal of Computer and Information Sciences, 1980.

[13] Liao, K., “Factors Affection Piston Ring Friction”, PhD thesis, Massachusetts Institute of Technology, 2013.

[14] Liu, Y., “Developing an Approach Utilizing Local Deterministic Analysis to Predict the Cycle Friction of the Piston Ring-pack in Internal Combustion Engines”, S.M. thesis, Massachusetts Institute of Technology, 2013.

[15] Lang, J., “Entwicklung eines Programms auf der Mehrkörpersystem-Modellanalyse zur Berechnung der Kolbensekundärbewegung unter

Berücksichtigung hydrodynamischer Schmierfilmeffekte am Kolbenschaft Diplomarbeit", Institut für Maschinenelemente und Maschinengestaltung, RWTH Aachen, 1992.

[16] Lang, J., "Kolben-Zylinder-Dynamik, Finite Elemente Bewegungssimulation unter Berücksichtigung strukturdynamischer und elastohydrodynamischer Wechselwirkungen", Dissertation RWTH Aachen, 1997.

[17] Suhara, T., Ato, S., Takiguchi, M., and Furuhama, S., "Friction and Lubrication Characteristics of Piston Pin Boss Bearings of an Automotive Engine," SAE Technical Paper 970840, 1997.

[18] Knoll, G.D. and Peeken, H,J, "Dydrodynamic Lubrication of Piston Skirts, Journal of Lubrication Technology", Transaction of the ASME, 104, 504-509, 1982.

[19] Zhu, D., Cheng, H., S., Arai, T. and Hamai, K., "A Numerical Analysis for Piston Skirts in Mixed Lubrication. Part I: Basic Modeling", Journal of Tribology, Transactions of the ASME, 114(3), 553-562, 1992.

[20] Zhu, D., Hu, Y.Z., Cheng, H. S., Arai, T. and Hamai, K., A "Numerical Analysis for Piston Skirts in Mixed Lubrication. Part II: Deformation Considerations", Journal of Tribology, Transactions of the ASME, 115, 125-133, 1993.

[21] Wong, V.W., Tian, T., Lang, H., Ryan, J.P., Sekiya, Y., Kobayashi, Y. and Aoyama, S., "A Numerical Model of Piston Secondary Motion and Piston Slap 143

in Partially Flooded Elastohydrodynamic Skirt Lubrication", SAE Paper 940696, 1994.

[22] Randall J. LeVeque, "Numerical methods for conservation laws", Basel, Boston: Birkhuser Verlag, 1992.

[23] Greenwood, J. A. and Tripp, J., "The Contact of Two Nominally Flat Surfaces", Proc. Inst. Mech. Engrs., 185, 625-633, 1971.

[24] Rebecca M Hoffman, Agus Sudjianto, Xiaoping Du and Joseph Stout, "Robust piston design and optimization using piston secondary motion analysis", SAE paper 2003-01-0148, 2003.

[25] Benoist Thirouard, "Characterization and modeling of the fundamental aspects of oil transport in the piston ring pack of internal combustion engines", PhD thesis, Massachusetts Institute of Technology, 2001.

[26] Baelden, C, "A Multi-Scale Model for Piston Ring Dynamics, Lubrication and Oil Transport in Internal Combustion Engines", PhD thesis, Massachusetts Institute of Technology, 2014.